Positron Lifetime Spectroscopy: Digital Spectrometer and experiments in SiC

Reino Aavikko

Laboratory of Physics
Helsinki University of Technology
Espoo, Finland

Dissertation for the degree of Doctor of Science in Technology to be presented with due permission of the Department of Engineering Physics and Mathematics for public examination and debate in Auditorium K at Helsinki University of Technology (Espoo, Finland) on the 29 th of June, 2006, at 13 o'clock.

Dissertations of Laboratory of Physics, Helsinki University of Technology
ISSN 1455-1802

Dissertation 141 (2006):
Reino Aavikko: Positron Lifetime Spectroscopy: Digital Spectrometer and experiments in SiC
ISBN 951-22-8242-9 (print)
ISBN 951-22-8243-7 (electronic)

Otamedia OY
ESPOO 2006

Abstract

A digital positron lifetime spectrometer has been designed, set up and tested comprehensively. The system consists of a fast commercial digitizer connected to a computer, a simple coincidence circuit and software to extract the timing from the collected detector pulses. The system has the same time resolution as a conventional analog apparatus using the same detectors. The pulse processing part of the spectrometer is able to analyze and store in real time several thousands of events per second, which is an order of magnitude more than the count rates in typical positron lifetime experiments. The data acquisition can handle small pulses, down to a few tens of millivolts, and its time scale linearity and stability are very good.

Positron spectroscopy has been used to study native vacancy defects in High Temperature Chemical Vapor Deposition grown semi-insulating silicon carbide. The material is shown to contain (i) vacancy clusters consisting of 4–5 missing atoms and (ii) Si vacancy related negatively charged defects. The growth of the clusters due to the annealing of the samples was observed. The total open volume bound to the clusters anticorrelates with the electrical resistivity both in as-grown and annealed material. It is concluded that Si vacancy complexes compensate electrically the as-grown material, but are suggested to migrate to increase the size of the clusters during annealing, leading to loss of resistivity.

Preface

This thesis has been prepared in the Positron Group in the Laboratory of Physics at the Helsinki University of Technology during the years 2002–2006. I am grateful to Prof. Pekka Hautojärvi for giving me the opportunity to work in this experimental group.

I am indebted to late Prof. Kimmo Saarinen for the excellent guidance and supervision he could provide me for the vast majority of time I was working in the laboratory. This thesis wouldn't exist without his enthusiasm and creativity. I am also glad for guidance and insight of Dr. Klaus Rytsölä especially in the regard of the instrumentation side of the thesis. Also, I would like to mention Dr. Jaani Nissilä, who had an active role in my work especially at the beginning of my thesis.

I wish to thank the members of the positron group, both current and former, for creating a pleasant and inspiring working environment. Also the help from the administrative staff and the skillful people at the electronic and mechanical workshops is gratefully appreciated. Acknowledgments belong also to my other collaborators outside the laboratory—especially to the people from Linköping University and Norstel AB, who have provided both samples for SiC measurements as well as their insight and understanding to the matter.

Finally, I wish to thank my parents, sisters and friends for all the support, encouragement and joy they have provided during the years.

The financial support from the Vilho, Yrjö and Kalle Väisälä foundation is gratefully acknowledged.

Helsinki, March 2006

Reino Aavikko

Contents

List of publications

This thesis consists of an overview and the following publications:

I K. Rytsölä, J. Nissilä, K. Kokkonen, A. Laakso, R. Aavikko and K. Saarinen *Digital measurement of positron lifetime,* Applied Surface Science, **194** (1-4) (2002) pp. 260-263.

II R. Aavikko, K. Rytsölä and J. Nissilä *Linearity tests of a Digital Positron Lifetime Spectrometer,* Materials Science Forum **445-446**, (2004) pp. 462-464.

III J. Nissilä, K. Rytsölä, R. Aavikko, A. Laakso, K. Saarinen and P. Hautojärvi *Performance analysis of a digital positron lifetime spectrometer,* Nuclear Instruments and Methods in Physics Research A **538** (2005) pp. 778-789.

IV R. Aavikko, K. Rytsölä, J. Nissilä and K. Saarinen *Stability and performance characteristics of a Digital Positron Lifetime Spectrometer,* Acta Physica Polonica A **107**, (2005) pp. 592-597.

V R. Aavikko, K. Saarinen, B. Magnusson, E. Janzén *Clustering of Vacancies in Semi-Insulating SiC Observed with Positron Spectroscopy,* Materials Science Forum: In print.

VI R. Aavikko , K. Saarinen, F. Tuomisto, B. Magnusson, and E. Janzén. *Clustering of vacancy defects in high-purity semi-insulating SiC,* arXiv:cond-mat/0603849

VII B. Magnusson, R. Aavikko, K. Saarinen, N.T. Son, E. Janzén *Optical studies of Deep Centers in Semi-Insulating SiC,* Materials Science Forum: In print.

The author has had an active role in all the phases of the research reported in this thesis. He has participated actively in the development and construction of the measurement instruments, planning and performing the experiments, analysis of the experimental data, and he has contributed significantly to the interpretation of the results. The author has taken part in the elaboration of the measurement system in Publication I. He has constructed the digital lifetime spectrometer and written the necessary computer codes as well as executed the experiments related to publications II–IV. The author has performed the measurements and data-analysis of Publications V-VI, including theoretical calculations of Publication VI. The author has participated in the positron-related measurements and data-analysis in publication VII. He has been the corresponding author of Publications II–VI.

Chapter 1

Introduction

Positron annihilation spectroscopy is an experimental method for studying vacancy-type defects in solid materials. Lately the most common materials investigated with the method have been semiconductors, metals and polymers. This thesis consists of development of the positron technique and application of the technique to study semiconductor materials. More specifically, the thesis consists of development of a digital positron lifetime spectrometer and of positron lifetime measurements applied to study High Temperature Chemical Vapor Deposited (HTCVD) silicon carbide.

Digital data readout techniques applied to nuclear radiation detectors have recently become viable as a result of the development of fast analog-to-digital converters (ADC). An early conversion to digital form both simplifies the measurement setup and enables various corrections to the data with software. Digital data collection methods have already been used in both pulse height and time-interval spectroscopies. Publications I-IV treat the application of the digital technique to construct a positron lifetime spectrometer.

Publication I presents a study on the possibility to set up a digital positron lifetime spectrometer. A digital oscilloscope is used to show for the first time that the concept is realizable. The performance characteristics (primarily resolution and count rate) of the spectrometer are poor due to the primitivity of the timing algorithms and the low suitability of the hardware, though.

In Publications II-IV a more advanced digital positron lifetime spectrometer is presented. The setup is described in detail and different characteristics of the spectrometer are studied extensively. It is shown that the performance of digital spectrometer is equal to or better than that of an analog spectrometer. The performance of the electronics and algorithms have reached the level, where the

limiting factor for the improvement of the performance of the system are the detectors rather than the timing electronics.

Silicon carbide (SiC) is a promising semiconductor material for high-temperature, high-power, high-frequency and radiation resistant applications. Semi-insulating SiC has shown great potential as a substrate material for SiC and III-nitride microwave applications. SiC substrates can be made semi-insulating by introducing deep levels (either impurities or intrinsic defects) to the material. Besides semiconductor applications, single crystalline SiC has found its way to gemstones - the material is sold with a brand name "Moissanite" and it is claimed that most of the properties of it are equal to those of diamond. Polycrystalline SiC has been available for decades and has been used mainly as abrasive. The High-Temperature Chemical Vapor Deposition (HTCVD) technique [1] uses pure gases to grow high-purity semi-insulating SiC. Native vacancies have been observed in the material in electron paramagnetic resonance experiments,[1–6] but their role in the electrical compensation is still unresolved. The publications V-VII involve studies of HTCVD grown silicon carbide.

In Publication V bulk HTCVD SiC has been studied using positron Doppler broadening spectroscopy. In this study it is shown that the as-grown material contains vacancy clusters. In Publication VI the material has been investigated using positron lifetime spectroscopy. Decomposition of the lifetime spectra and comparison of the results with theoretical calculations allowed to estimate the sizes of these clusters - approximately 3-4 atoms in the as-grown material. The clusters are seen to grow to sizes of more than 30 atoms due to high temperature annealing. In addition to the clusters also smaller vacancy type defects are detected. The defects are found to be negative and they are especially prominent in samples grown under Si poor environment. It is also shown that in this material the open volume of these vacancies are larger than that of V_{C}. Therefore they are identified as V_{Si}-related defects. Publication VII involves characterization of the material with different techniques: optical (absorption, photoluminescence), secondary ion mass spectroscopy and positron annihilation. In the publication it is verified that the concentration of the residual impurities is low: $< 10^{15}$ cm^{-3}. The material is also shown to contain V_{Si}, the concentration of which lowered during the annealing.

Chapter 2

Positron Spectroscopy

Positron annihilation spectroscopy is an experimental method sensitive to defects with open volume on atomic scale. The method is based on the detection of the radiation produced in the annihilation of positrons (i.e. anti-electrons) with the electrons in the material studied. Prior to annihilation, positrons can get trapped at vacancy defects due to the missing Coulomb repulsion of the positive ion core. At a vacancy defect the electron density is lower than in the bulk material, and thus the lifetime of a positron trapped into a vacancy is longer than that of a positron in the lattice. Hence, the positron lifetime reflects the open volume of the defects in the material. In addition to the lifetime measurements, other positron measurements include Doppler broadening of the annihilation radiation and the angular correlation of annihilation radiation (ACAR). In these methods the momentum of the annihilating electrons are measured indirectly. Thus they give information on the chemical environment of the vacancies in the material. Thorough reviews on the measurement methods and the theory of positrons in solids can be found in e.g. Refs. [7–9].

2.1 Lifetime measurements

The positron lifetime measurements presented in this thesis have been carried out using fast (i.e. unmoderated) positrons, obtained directly from β^+ active ^{22}Na source. The studied samples (two identical pieces needed, typical size is $\approx 5 \times 5$ mm^2) are sandwiched around a positron source (typically $\approx 5 - 50$ μCi) deposited on folded thin metal foil (typically 1.5 μm thick Al, area $\approx 3 \times 3$ mm^2), in such a way that the emitted positrons immediately hit the samples regardless of the direction of their emission. The sample-source sandwich is then placed between two detectors in a collinear geometry. Both detectors consist of a fast

scintillator coupled to a photomultiplier tube. In the decay of a ^{22}Na nucleus, a 1.275 MeV γ quantum is emitted simultaneously with the positron. Detecting this quantum allows determination of the time of birth of the positron. The annihilation time instant is determined by detecting a 511 keV γ-quantum emitted at the annihilation of the positron. A rather low activity of the positron sources allows distinguishing the start and stop pulses arising from the same event, as generally there is only a single (or no) positrons in the sample at a given time. The average time difference between positron emissions in a customary positron source is approximately a microsecond, whereas the typical positron lifetimes are in the range of 0.1–1 nanoseconds. The positrons are emitted from the ^{22}Na source with a continuous energy distribution with maximum energy of 540 keV. For instance, for silicon carbide this results in average penetration depth of 80 μm, meaning that the positrons effectively probe the bulk of the material, as typical positron diffusion lengths are three decades shorter.

The γ quanta are observed with the scintillation detectors, whose pulses are processed either in conventional (analog) way or digitally (see chapter 3). In the analog setup, constant fraction discriminators are used for timing the detector pulses, and a time-to-amplitude converter and a multi channel analyzer are used for determination- and histogramming of the time-intervals. In the digital setup, the pulses of the detectors are directly digitized and the timing information from the pulses is extracted using software. Typically $1 - 5 \times 10^6$ pulses are collected to a single lifetime spectrum. This takes $1 - 10$ hours depending on the activity of the source and the measurement geometry.

The positron lifetime spectrum is the probability of an annihilation at time t. If positrons have several different states from which to annihilate, the lifetime spectrum is

$$-\frac{\mathrm{d}n(t)}{\mathrm{d}t} = \sum_i I_i e^{-\lambda_i t}, \tag{2.1}$$

where λ_i are the decay constants and I_i the corresponding intensities ($\sum_i I_i = 1$). The lifetime components are defined as the reciprocal values of the decay constants $\tau_i = \lambda_i^{-1}$.

Examples of measured lifetime spectra are presented in Fig. 2.1. The measured spectra are convolution of the ideal exponential spectrum presented in equation 2.1 and the resolution function of the system. Typical Full Width at Half Maximum (FWHM) of the resolution function is around 200–250 ps (depending mainly on the sizes of the scintillators and the energy windows used) and its ideal shape is Gaussian.

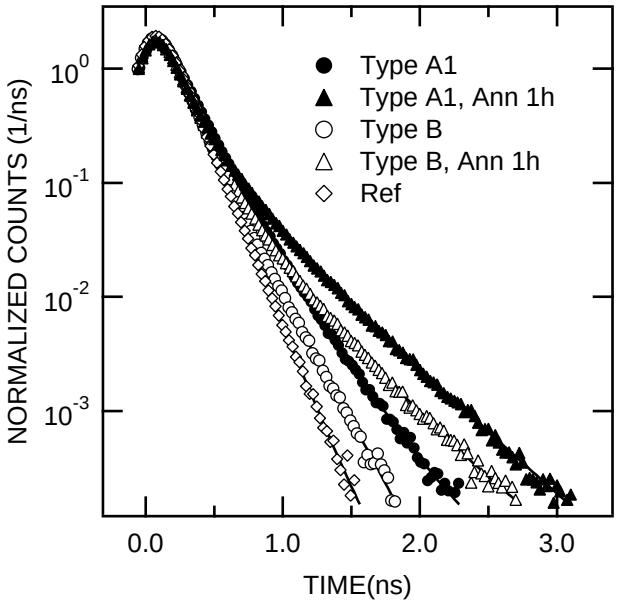

Figure 2.1: Positron lifetime spectrum measured with the digital positron lifetime spectrometer in different samples of bulk SiC. The spectra are source- and background corrected.

In addition, a few percent of the positrons annihilate in the source material and the Al foil surrounding it, producing additional components to the experimental spectrum. For these reasons, usually at most three components can be reliably separated in the experimental lifetime spectra. The separation is normally performed by fitting the convoluted theoretical lifetime spectrum to the measured data. The effect of the source components can be eliminated by measuring a defect free reference sample. On the other hand, when the resolution function is Gaussian, it does not affect the average positron lifetime defined as

$$\tau_{\mathrm{ave}} = \sum_i I_i \tau_i = \int_0^\infty tP(t)\mathrm{d}t. \tag{2.2}$$

The average positron lifetime (equal to center of mass of the spectrum) is an important quantity since it can be always determined even if the decomposition of the lifetime spectrum is difficult.

2.2 Positron Trapping

When energetic positrons are implanted to the sample material, they rapidly lose their kinetic energy due to ionizations, electron excitations, phonon emissions etc. This process is called thermalization. In crystalline solid the thermalization proceeds to a delocalized (free) Bloch-like state. The possible vacancy type defects in the lattice, are perceived by the positron as potential wells, whose binding energies are typically a few eV - significantly larger than the thermal energies. The positrons can get trapped to these defects. The transition from the free (Bloch-like state) to the localized state is called positron trapping.

In the conventional positron trapping model [7, 9] it is assumed that at time-zero all positrons are free in the bulk lattice. The trapping rate κ of positrons to the traps with concentration c is then linearly dependent on the concentration of the traps as $\kappa = \mu c$, where μ is the positron trapping coefficient to the traps. Typical trapping coefficients for negative vacancies in semiconductors are in range $0.5..5 \times 10^{15}$ s^{-1}. [7] For neutral vacancies the trapping rates are less: for example the trapping coefficients of the neutral and negative mono- and divacancies in Si have been found to differ by a factor of 1.5-3.5. [9–11]

In semiconductors the positron trapping coefficient depends on temperature and the charge state of the defect. In neutral vacancies the temperature dependence of the trapping is non-existent, but the trapping coefficient of negative traps increases as the temperature decreases. In principle the trapping coefficient for positive vacancies should increase as a function of temperature. However the positron trapping to the positive vacancies is very weak: positive vacancies cannot generally be detected with positrons. The temperature dependence of a negative trap varies as $T^{-0.5}$. Additionally, positrons can get trapped also at hydrogen-like Rydberg states surrounding negative ion type defects (shallow traps for positrons). The trapping rate to the Rydberg state μ_R varies also as $T^{-0.5}$, which is the result predicted by theory for the transition from a free state to a bound state in a Coulomb potential. The binding energies of positrons trapped to the Rydberg states are typically 0.01-0.1 eV, meaning that the trapped positrons can escape from these states due to thermal fluctuations. The presence of negative ions can then be observed as decrease of average positron lifetime at low temperatures, as the negative ions compete with vacancy defects in positrons trapping.

In case the samples contain only one vacancy type positron traps (which are deep, i.e. no detrapping due to thermal fluctuations) with positron lifetime τ_D, the positrons have two different states from which to annihilate (bulk and defect). The longer experimental lifetime component will be equal to that of the positron lifetime in the defect, i.e. $\tau_2^{\text{exp}} = \tau_D$. Because of the positrons trapping away from the bulk at rate κ, however, the positrons spend less time in the bulk than would

be the case in the absence of the trapping. Thus the shorter experimental lifetime component $\tau_1^{\mathrm{exp}} = (\tau_\mathrm{b} + \kappa)^{-1}$ will be lower than the lifetime in bulk material τ_b. This effect can be used to test, whether the one-trap-model is sufficient to explain the measured data. If only one type of vacancy defects are present, lifetime τ_1 is related to $\tau_\mathrm{ave}, \tau_\mathrm{b}$ and τ_2 as [7, 12]

$$\tau_1^{\mathrm{TEST}} = \tau_\mathrm{b} \left(1 + \frac{\tau_\mathrm{ave} - \tau_\mathrm{b}}{\tau_2 - \tau_\mathrm{ave}} \right)^{-1} = \tau_\mathrm{b} \left(\frac{\tau_2 - \tau_\mathrm{ave}}{\tau_2 - \tau_\mathrm{b}} \right). \tag{2.3}$$

If the samples contain only one vacancy type positron traps (i.e. if equation 2.3 holds), the positron trapping rate can be determined from the measured lifetime components as

$$\kappa = \frac{I_2}{I_1}(\lambda_\mathrm{b} - \lambda_D) = \frac{\tau_\mathrm{ave} - \tau_\mathrm{b}}{\tau_\mathrm{D} - \tau_\mathrm{ave}} \frac{1}{\tau_\mathrm{b}}. \tag{2.4}$$

Sometimes - if the samples contain more than two positron states (e.g. two different vacancy type positron traps and the bulk), it might not be possible to separate all positron lifetime components. If the two shorter (physical) lifetime components are intermixed (this might be the case e.g. if the samples contain vacancy clusters with lifetime τ_CL and small vacancy-type defects with positron lifetime τ_V, whose lifetime is intermixed with the positron lifetime in bulk τ_b), the positron trapping rates can be extracted as

$$\kappa_\mathrm{V} = \frac{\tau_1(\tau_\mathrm{b}^{-1} - I_2\tau_2^{-1}) - I_1}{(\tau_\mathrm{V} - \tau_1)}, \tag{2.5}$$

$$\kappa_\mathrm{CL} = \frac{I_2}{I_1}(\tau_\mathrm{b}^{-1} - \tau_\mathrm{CL}^{-1} + \kappa_\mathrm{V}), \tag{2.6}$$

where τ_1 and τ_2 are the shorter and longer experimentally separated positron lifetime, respectively. From the kinetic equations of the positron trapping model it is possible to solve also trapping rates to more complicated trapping systems than presented here. However application of these trapping models is usually impractical, as the number of different lifetime components that can typically be decomposed is two to three.

Chapter 3

Digital positron lifetime spectrometer

Positron lifetime is measured by detecting the time difference between the γ-quantum created in coincidence with the birth of the positron and a γ-quantum created at the annihilation. These quanta are detected with two fast scintillation detectors. In the digital spectrometer the pulses of the detectors are directly digitized and the timing and energy windowing are then performed with software. Hence, the digital spectrometer replaces the conventional analog timing electronics (TAC, CF-DICSs). Before positron lifetime measurements, digital data readout techniques applied to nuclear radiation detectors have been used in pulse-height (see e.g. [13] and references therein) and time-interval spectroscopies. [14–16]

The first generation digital positron lifetime spectrometer was implemented using a digital oscilloscope connected to a computer using a GPIB-ethernet connection [Publ. I]. The concept was shown realizable, but because of the primitivity of the algorithms and unsuitability of the hardware the performance of the system was rather low.

The second generation of digital spectrometers use either a digital oscilloscope with internal hard disk [17–19] or a digitizer card directly connected to a computer [Publ. II-IV]. [20] These solutions allow coincidence rates that are practically unhindered by the electronics during the measurements. However, the pulse data analysis of the two realizations [17–20] is only possible "offline" (*i.e.* after the measurement), whereas the pulse processing of the setup constructed in this thesis is possible also "on-line" (*i.e.* during the measurement) [Publ. II-IV].

The setups presented in [17–20] use more than one digitizer channels, allowing the use of a highly resolution-optimized detectors with BaF_2 scintillators (the long

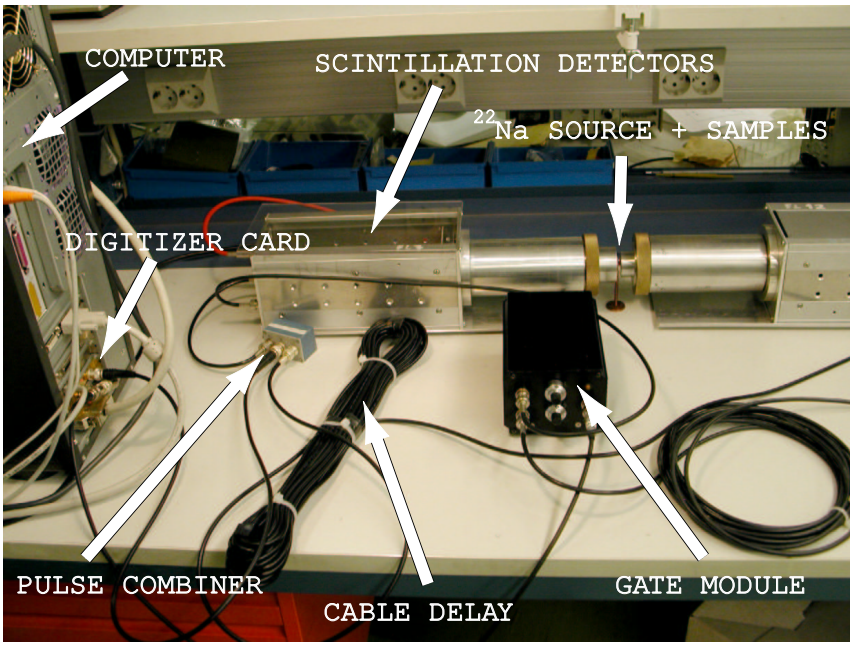

Figure 3.1: Photograph of a digital positron lifetime spectrometer set up at HUT/Lab. of Physics [Publ. IV]

tails of BaF_2 pulses prevent connecting more than one detector in single channel). The resolutions obtained with these systems have been 130..145 ps (using two-detector setups). Also possibility of using more than two detectors in the measurements (e.g. to capture both 511 keV γ-quanta) has been demonstrated in [17–19]). The setup presented in this thesis uses a single-channel digitizer and two detectors with plastic scintillators. Typical count rates of the system have been 200 1/s and resolution 220 ps with normal measurement geometries and source activities.

3.1 Hardware

Two fast scintillation detectors capture the $\gamma-$quanta which are emitted at the time of the birth and the annihilation of the positron. The anode pulses from the photomultiplier tubes (PMT) are led to a digitizer unit. The time information is then extracted from the voltage sample sequences with software.

A photograph of the spectrometer is presented in fig. 3.1 and the block diagram in fig. 3.2. The anode pulses are fed into a combiner and led via a single cable to the digitizer. To avoid timing errors arising from the ringing of the baseline after

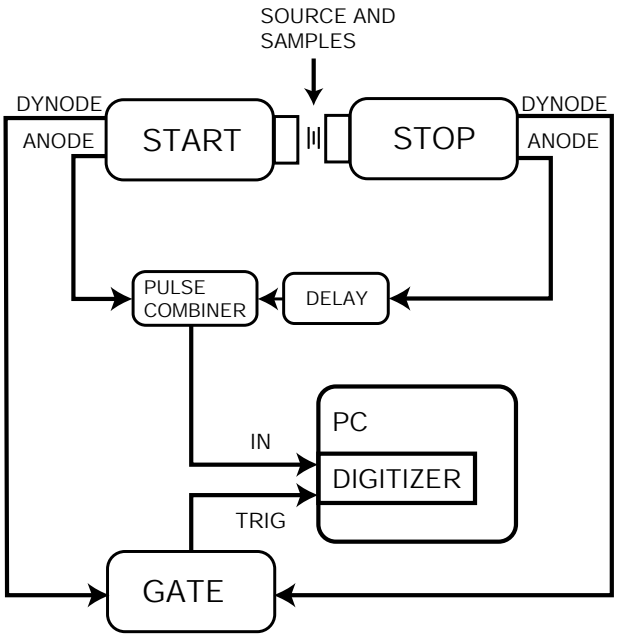

Figure 3.2: The figure shows block diagram of a digital positron lifetime spectrometer (see also photograph in fig. 3.1). [Publ. III]

the first pulse, a proper minimum delay (typically 50–100 ns) must be set between the pulses with a cable. The pulse combiner used in this case is Mini Circuits ZSC-2-1W (1-650 MHz) impedance matched pulse combiner (power splitter). The presented approach has two virtues: first, it allows using two detectors with just one digitizer channel, and second, the possible time spread related to the synchronization of the channels is not introduced between the start and stop pulses. The drawback of the approach is that in practice it prevents using BaF_2 as the scintillator material, as the long tail of the BaF_2 pulses in the start detector would sum up with the pulses of the stop detector.

In a typical positron lifetime spectrometer, the ratio of the true coincidence rate to the singles rate is only a couple of per cent. From the point of view of the data transfer into the computer, it is important to eliminate most of the non-coincident pulses. A sufficiently flexible triggering function has not yet been implemented in commercial fast digitizers. Hence, an external gate module to provide a triggering signal to the digitizer in case of a useful event was designed and constructed. The gate module gives an output signal if two negative pulses exceeding chosen amplitudes appear at the unit inputs within a selected time interval.

The digitizer used in this study is an 8-bit digitizer card DP210 by Acqiris. The

card is connected to the PCI-bus of the measurement computer. The bandwidth of the card is 500 MHz and its maximum sampling rate 2 GS/s. The card allows fast transfer of data from the buffer memory (up to 8000 events in on-board extended memory) to the computer memory.

The detectors of the spectrometer studied here were composed of fast plastic cylindrical scintillators (NE-111) and XP2020 photomultipliers (by Photonis). The sizes of the scintillators were $\Phi 30 \times 20$ mm^3 in both the start and stop detector (set for the capture of the 1275 keV and 511 keV $\gamma-$quanta, respectively).

With these detectors a typical count rate at ≈ 1 cm inter-detector distance (configuration allowing e.g. the use of a cryostat for sample cooling) is 200 1/s with a customary used 30 μCi ^{22}Na source. The count rate at a given source activity naturally depends strongly on the measurement geometry. In the tests described below, the count rate has typically been 50-200 1/s using 5-30 μCi sources.

With these detectors time resolution of the spectrometer was ≈ 220 ps, as will be shown in the following. This resolution is similar to that of typical analog spectrometers (with similar detectors) used at the Laboratory of Physics.

3.2 Software and Data Acquisition

The program for the Acqiris DP210 digitizer control and data collection was written in C++ using Microsoft Visual C++ 5.0. The software could be well run in a computer with a 500 MHz Pentium III Processor and 128 MB system RAM. However, after the initial tests a computer with dual AMD Athlon MP 1900+ processors was used. The multitasking program simultaneously controls the data acquisition and analyzes the data. This solution reduces the dead time in a usual positron lifetime measurement to a negligible level ($< 1\%$), where it is determined only by the transfer time of the data and the triggering rate of the digitizer.

3.2.1 Gains, digitizer FSR and energy windows

In the digital system the detector gains are set as follows: in order to utilize the Full Scale Range (FSR) of the digitizer most efficiently, the Compton continua of the 1.275 MeV and 511 keV γ-quanta should fill the FSR of the digitizer, as shown in figure 3.3. This is realized by setting the gains (i.e. HV) of the detectors suitably. As shown in the figure, this also means that the pulses corresponding to the upper part of the 1.275 MeV Compton continuum exceed the digitizer range in the stop detector.

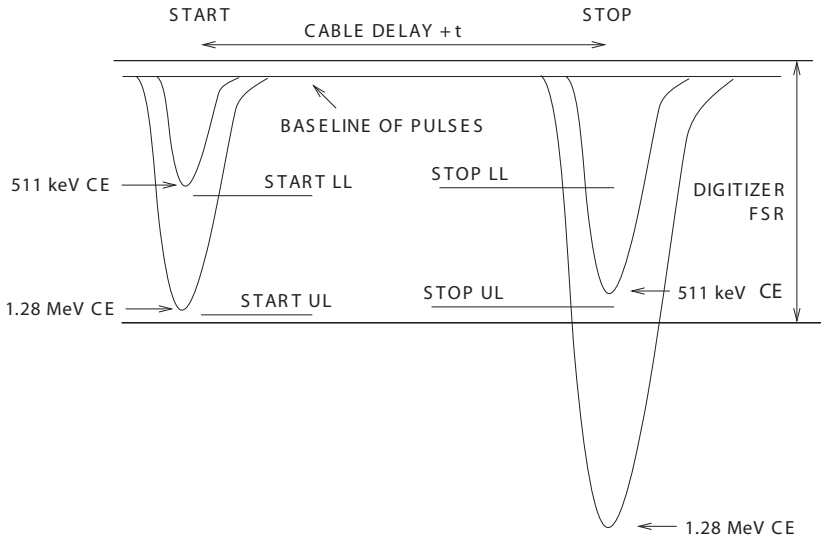

Figure 3.3: Schematic diagram on setting the gains for the two detectors (setup as in Fig. 3.2). In the figure are presented the two anode pulses as seen e.g. in the oscilloscope program of the digitizer (AcqirisLive), when the digitizer is triggered by the output of the gate module and a suitable (typically negative) trigger delay is set. The detector gains were set so, that the start detector anode pulses from the 1.28 MeV Compton edge (CE) fit the digitizer full scale range (FSR) and the pulses from 511 keV Compton edge fit the FSR in stop detector. Setting the gain this way causes 1.28 MeV pulses to exceed the digitizer FSR in stop detector. In the figure 't' is the lifetime of a particular positron.

When the gains are set, the energy windows are set in the same fashion as in analog apparatuses, i.e. as the relative amplitude (e.g. 50%) from the upper levels (set at the Compton edges of the corresponding γ quanta). After setting the energy windows, the optimal parameters for extraction of the timing information are obtained by repeatedly analyzing the same set of saved (typically ^{60}Co) data with different fitting parameters and by choosing the best values on the basis of the resulting coincidence spectra. For example, the dependence of the resolution as a function of the constant fraction in the timing is shown in figure 3.4 (see section 3.3.2 for details on the constant fraction timing method).

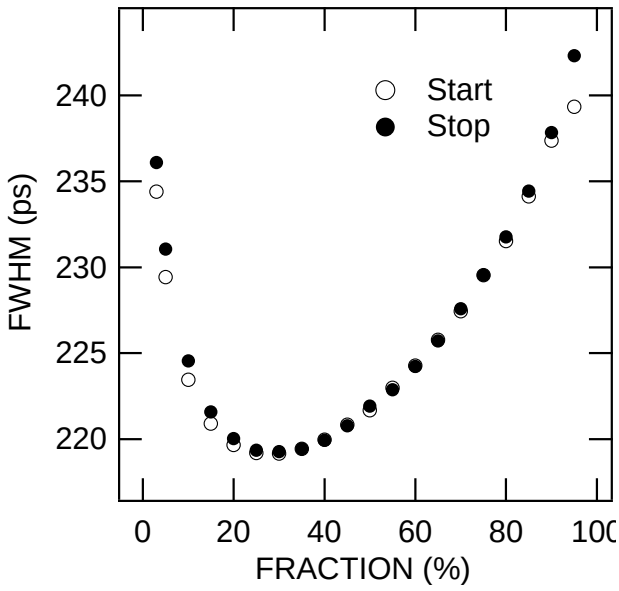

Figure 3.4: The time resolution of the spectrometer as a function of the fraction f_{CF} used in the constant-fraction timing (see section 3.3.2). [Publ. III]

3.3 Data analysis

A typical positron lifetime event is shown in Fig. 3.5. This sample sequence has been acquired with the Acqiris DP210 digitizer operating at a sampling rate of 2 GS/s. The first pulse originates from the 1.275 MeV $\gamma-$quantum and the second from the 511 keV annihilation photon.

The data analysis of one sweep consists of (i) checking that the sweep contains exactly two anode pulses (ii) checking that these pulses have correct amplitudes (i.e. they fit in the predetermined amplitude ranges) (iii) extracting the timing information from the pulses and (iv) histogramming the time intervals.

Checking the number of anode pulses (i) and their amplitudes (ii) are discussed in the next section. Several different timing methods (step iii) have been implemented in this thesis (see section 3.3.2). After the timing information of the two anode pulses has been extracted, histogramming the time intervals (iv) is trivial and the bin width (i.e. time channel width, typically 10–30 ps) can be arbitrarily chosen.

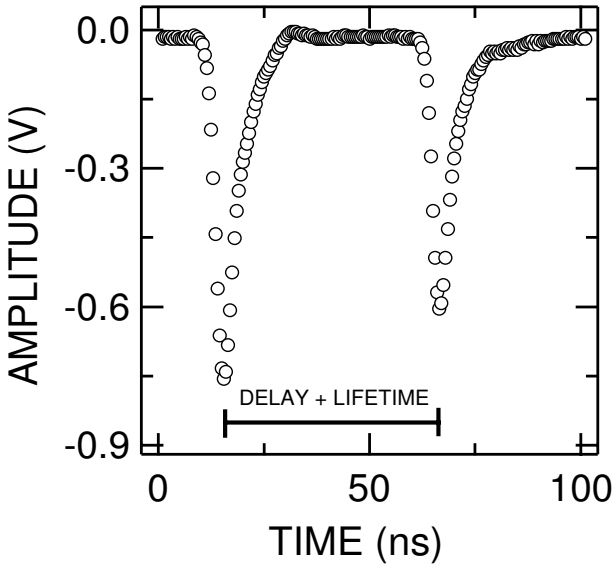

Figure 3.5: A typical positron lifetime event (sweep) as registered by the digital apparatus at 2 GS/s sampling rate. The first pulse in the graph originates from the 1.28 MeV γ quantum (in the start-detector) and the second one from the 511 keV annihilation photon (stop-detector). The two pulses are separated by the cable delay and the lifetime of this particular positron. [Publ. III]

3.3.1 Checking that the sweeps contain exactly two pulses of correct amplitudes (steps i, ii)

The amplitudes of the detector pulses correspond to the energies the γ-quanta have deposited to the detectors. These energies allow one to deduce the origin of the pulses even when the quanta have gone through Compton-scattering (a case typical when using plastic scintillators): If the deposited energy is higher than the energy corresponding to the Compton edge of 511 keV, the quantum originates from the 1.28 MeV quantum. Pulse amplitudes (energies) lower than this can in principle originate either from 1.28 MeV or 511 keV γ-quanta. However, in case the two pulses are detected in coincidence and one of them originates from 1.28 MeV quantum, the second one must by exclusion originate from 511 keV quantum. (This holds, if the coincidence is "true" i.e. the start and stop signals arise from the decay of the same ^{22}Na nucleus.)

Each digitized sweep is checked to assure that it contains exactly two pulses (one is not sufficient for timing and third might be e.g. a random coincidence. This is accomplished as follows (*minPeakHeight*, *start LL*, *start UL*, *stop LL* and *stop UL* are input parameters of the analysis program. *amplitude1, amplitude2* and

amplitude3 are variables in the analysis program:

1. Position of the highest amplitude of the sweep is searched. This amplitude is stored to *amplitude1*.
2. Area of predetermined length (in sampling points) is blocked around the position found in step 1. (The blocked length is chosen in advance to be equal to the anode pulse length.)
3. Highest (amplitude) point of the remaining (unblocked) sweep is searched. This amplitude is stored to *amplitude2*.
4. Area of predetermined length is blocked around the position found in step 3.
5. The highest amplitude of the remaining sweep is searched. This amplitude is stored to *amplitude3*.
6. Check that *amplitude1* $>$ *minPeakHeight* and *amplitude2* $>$ *minPeakHeight*. If this is not the case, the sweep contains less than two usable pulses and the sweep is discarded.
7. Check that *amplitude3* $<$ *minPeakHeight*. If this is not the case, sweep contains more than two pulses and the sweep is discarded.
8. Check that the amplitudes of the two pulses fit the predetermined energy windows *start LL* $\leq$ *firstPulseHeight* $<$ *start UL*, and *stop LL* $\leq$ *secondPulseHeight* $<$ *stop UL*, where *firstPulseHeight* and *secondPulseHeight* are the amplitudes of the two pulses found (i.e. *amplitude1* and *amplitude2*) in temporal order in the sweep.

3.3.2 Pulse Timing (step iii)

After checking the number of anode pulses in the sweep (i) and their amplitudes (ii) the next step in the analysis is to determine the timing instants corresponding to the two anode pulses. The lifetime of the particular positron (plus constant delay due to cables and PMT:s) is then the difference between the timing instants of the two anode pulses. For example, the functioning of the timing is demonstrated in Fig. 3.6. In the figure one is able to perceive the time-spread associated to the detectors.

The different timing methods implemented in this thesis are presented in following. The methods are compared by testing them with a single set of data. Note that the resolutions presented in the following are not universal for the algorithms presented, as the figures depend on the energy windows and the detectors used.

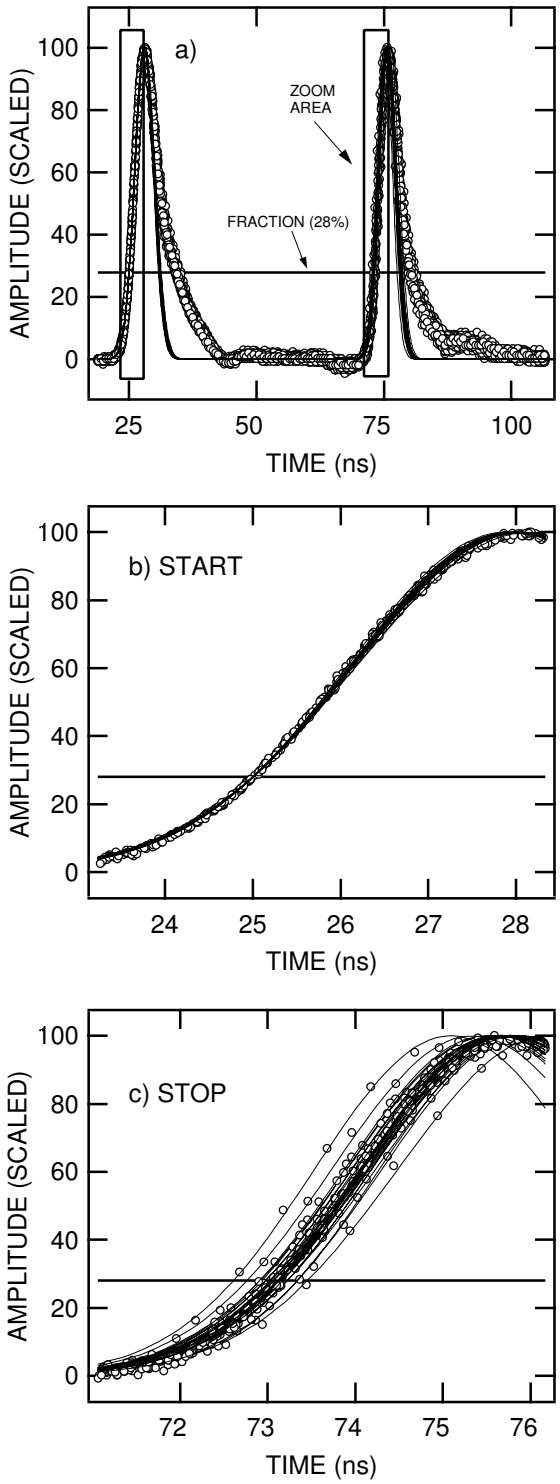

Figure 3.6: A timing demonstration. The pulse pairs (panel **a**) are obtained by measuring ideal coincidence source. A constant fraction method using a Gaussian fit has been used for timing (section 3.3.2). Used constant fraction (28%) is shown as vertical line. Pulse pairs have been shifted and pulse heights normalized so that the timing instants of *start*-pulses coincide (panel **b**). The time resolution can then be observed as the jitter of the positions of normalized *stop*-pulses at the constant fraction level (panel **c**). [Publ. III]

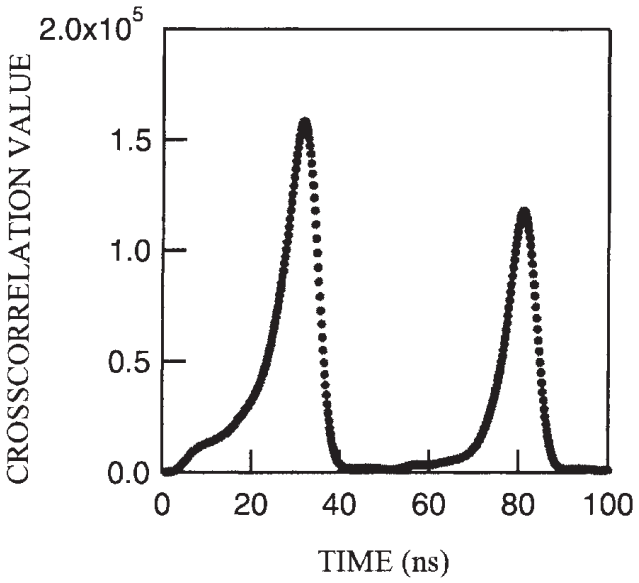

Figure 3.7: Example of a cross correlation curve in which a model pulse has been cross correlated with the sweep. The timing instants of the two anode pulses correspond to the two peaks. [Publ. I]

Timing from Anode pulse maximum

The simplest possibility of determining the position of an anode pulse is simply using the (time) position of a sampling point, whose amplitude is highest. Problems related to this method are obviously that (i) the timing accuracy is limited by the sampling period and (ii) that even if the position of the anode pulse maximum is measured with perfect accuracy, this might not be the optimal timing instant in regard with the incident γ quantum. With this method the FWHM has been around 530 ps.

Cross Correlation

In this method, a cross correlation is calculated between the digitized anode pulse (V_{ADC}) and a model pulse (V_{MP}). The model pulse can be obtained by averaging several anode pulses. Cross correlation value is defined as

$$XC(i) = \sum_{j=1}^{|V_{MP}|} V_{ADC}(i+j) \cdot V_{MP}(j), \tag{3.1}$$

where "$\cdot$" denotes the *inner product*. The sum is calculated up to the length of the model pulse vector (equal to the length of the model pulse $|V_{MP}|$). After

calculating the cross correlation curve, a parabola is fitted to the peak of the cross correlation curve XC. The location of this peak is then taken to be the timing instant. Best resolutions obtained with this timing method have been around 240 ps.

Center of mass (COM)

The center of mass of anode pulse is determined as

$$T = \frac{\sum_{t=t_0}^{t_f} V_t \times t}{\sum_{t=t_0}^{t_f} V_t}, \tag{3.2}$$

in which V_t is the digitized value at time t. Here the limits of the summation t_0 and t_f are chosen as the time instants, when the anode pulse height is over a given constant fraction of the pulse maximum height. The best time resolutions with the method have been around 250 ps (with 50 % Co-energy windows).

Constant Fraction (CF) Methods

In the constant fraction methods, the timing instance of an pulse is obtained as a position which corresponds to a constant fraction (often 20-50%) of the full height of the pulse. In analog systems this processing has been realized by clever summation of suitably delayed and attenuated (and/or inverted) replicas of the original pulse and by monitoring the zero-crossing of the result.

In digital spectrometer the position of the Constant Fraction can be obtained in a more straightforward manner by first determining the height of the anode pulse and then by searching "backwards" for the time instant, whose amplitude corresponds to the predetermined constant fraction of the pulse height.

A complication in the digital realization is that the sampling interval is long compared to the accuracy needed for determining the positions of the anode pulses (e.g. with 2 GHz sampling frequency the sampling interval is 500 ps, whereas the needed timing accuracy is around 50 ps or less). This means that the leading edge of the anode pulse needs to be interpolated or some other fitting or filtering method needs to be applied in order to allow the determination of the constant fraction with an accuracy better than one sampling interval. The different strategies tried for this are (obtained resolutions in parenthesis)

- Linear interpolation (260 ps)
- Fitting of Gaussian function (220 ps)

- Spline interpolation of a moving average (220 ps)
- Smoothing spline (220 ps)

The simplest strategy for searching the position of the constant fraction was linear interpolation between successive sampling points of the anode pulse. With this method the best results were obtained when the constant fraction has been around 40 % of the pulse height. In this case the FWHM of the resolution function was 260 ps.

The Gaussian function was found to describe the shape of the leading edge of an anode pulse rather well. The implemented constant fraction method exploits this observation by obtaining the instant of the constant fraction analytically from the fitted parameters. The fitting of the Gaussian function was realized either by *grid search* [21] or by *Levenberg-Marquardt* [22] method. The realization of the *Levenberg-Marquardt* method was found to be computationally faster, but less robust (i.e. the fitting fails in more cases than in the Grid Search leading to loss of a small fraction of measured pulses). The time resolutions obtained with both methods have been approximately 220 ps.

A possible method for smoothing the leading edge of anode pulse is by calculating a (weighted) moving average over the sampled anode pulse. After this the calculated moving average curve is interpolated with normal splines and the constant fraction is obtained from this interpolated curve. The best resolutions with the method have been ≈220 ps. This method has been first proposed in [17].

The leading edge can be smoothed also by calculating a *smoothing spline* [23] from the anode pulse. The constant fraction is then obtained from this curve. Smoothing spline fitting minimizes the cost functional

$$f(s) = p\sum_i (s(x_i) - y_i)^2 + (1-p)\int s''(x)^2 dx, \tag{3.3}$$

in which $s(x)$ is a spline, (x_i, y_i) digitized samples and p a smoothness parameter. [24] This method is nowadays commonly used at HUT, since the best time resolutions have been obtained with it, and it does not involve apriori assumptions on the exact shape of the anode pulses (as e.g. fitting a Gaussian function does). Best resolutions have been FWHM = 220 ps.

The similarity of the obtained resolutions and the results from the simultaneous measurements with an analog setup (see section 3.4.2) suggest that all three timing algorithms are near the optimum for constant fraction methods.

3.4 Performance of the system

Typically the two most prominent performance characteristics of a lifetime spectrometer are its resolution and count rate. Improved resolution helps decomposing positron lifetime spectra into different components and higher count rates allow faster measurements. The count rate helps also in the decomposition, due to the availability of better statistics. In many cases it is advantageous to collect a higher number of counts with lower resolution (if the available measurement time is fixed) [25], as typically there is a tradeoff between count rate and resolution (e.g. by changing energy windows or scintillator sizes). Besides resolution and count rate, other important performance characteristics include linearity of the time base (important for correctness of the results), stability of the spectrometer (for longer measurement times) and performance with small pulse amplitudes (small pulse amplitudes improve the long-term stability of the system). In the following is presented a summary of different performance tests run on the spectrometer. It will be shown that the performance of the system is equal to- or better than the performance of the conventional analog spectrometers.

3.4.1 Pulse processing

In order to investigate the maximum count rate of the system, transfer- and pulse processing rate tests were made. In a test in which pulses were fed to the digitizer from a pulse generator, up to 30,000 unprocessed events per second could be recorded to the computer main memory. This rate is limited by the hardware. When performing an online analysis to the data, the computing power of the processor limits the maximum rate of true analyzed events to 3,000 1/s (using cubic smoothing spline fitting). This rate is clearly high enough for positron lifetime measurements, as typical count rates in the measurements are around 200 s^{-1}.

3.4.2 Time resolution

The time resolution of the spectrometer measures the accuracy with which the spectrometer can measure an ideal coincidence peak. In analog systems it is widely accepted that the electronics degrades the total resolution only marginally, by around 10 ps or less at the 200 ps level. In other words, the resolution of a spectrometer with properly optimized electronics is determined by the detectors. In a digital spectrometer the 'electronic resolution' is influenced by several factors: e.g. the sampling rate (or the number of samples in the pulse), the noise added to the voltage pulse by the digitizer, and the amplitude linearity of the digitizer. All the following data in this section are analyzed using the Gauss-fit procedure.

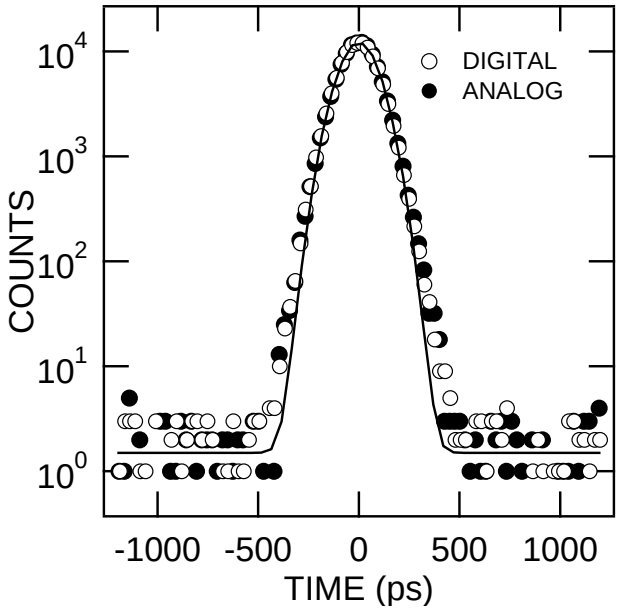

Figure 3.8: Resolution functions obtained with analog and digital timing. The same detector pulses have been processed with both systems. This has been realized by splitting the detector anode pulses. Both spectra contain ≈ 110000 counts. The number of coincidences in the digitally measured spectrum is more than 98% of the coincidences processed by the analog system (the digital system discards events with more than two pulses). The bin width of the digital system has on purpose been chosen to be equal to that of the analog apparatus (25.65 ps/ch). [Publ. III]

The timing performance of the digital positron lifetime spectrometer was tested by comparing it with an well-tuned analog spectrometer. The analog electronics was composed of units which were known to work well (Ortec Model 583 differential CFDs, Ortec 566 TAC). The digitally collected pulses, sampled at 2 GS/s, were analyzed using the smoothing spline method with $p = 0.3$ and $f_{\mathrm{CF}} = 0.2$.

To assure reliable comparison, the *same events* were handled with both systems. This was accomplished by dividing the anode pulses with impedance matched power splitters to the constant fraction discriminators and the pulse combiner of the digital system. The digitizer was then triggered with the analog 'Valid Conversion' output of the TAC.

The data acquired with the two systems are shown in Fig. 3.8. Closed markers represent the data processed with analog timing electronics and open ones the digitally processed data. No difference is noticeable. The FWHM is 212 ps for both sets of data ($\approx 60\%$ ^{60}Co energy windows used). The line presents a

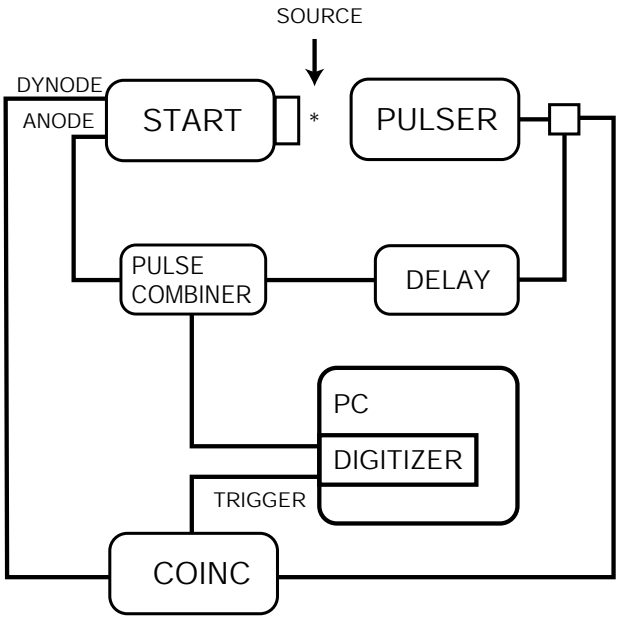

Figure 3.9: Block diagram depicting setup (ii) used for measuring the linearity of the digital spectrometer. In the setup a random time instant is obtained from a radioactive source, and a periodical stop-signal from the pulser. This results in even time distribution. The triggering module is used for detecting events, where the start signal is detected in a suitable time frame compared to the stop signal.

Gaussian fit. Evidently, the contribution of the electronic resolution is negligible in both cases.

3.4.3 Linearity of the time base

The linearity of a positron lifetime spectrometer was measured by introducing random start- and periodic stop signals. [26] This results in a uniform distribution of the time intervals. The start pulses are obtained from a radioactive source and the stop pulses from a pulser.

The different setups used for measuring the time linearity of the spectrometer are firstly (i), both start- and stop pulses are combined, separated by a cable delay and run on the same channel. The digitizer is then triggered simply from the measured channel. The delays are adjusted so that the stop pulse will be at the end of the sweep assuring that it will be interpreted correctly by the analyzing software. This setup yields much unneeded data which slows down the measurement, since the ratio of coincidences with triggered sweeps is low.

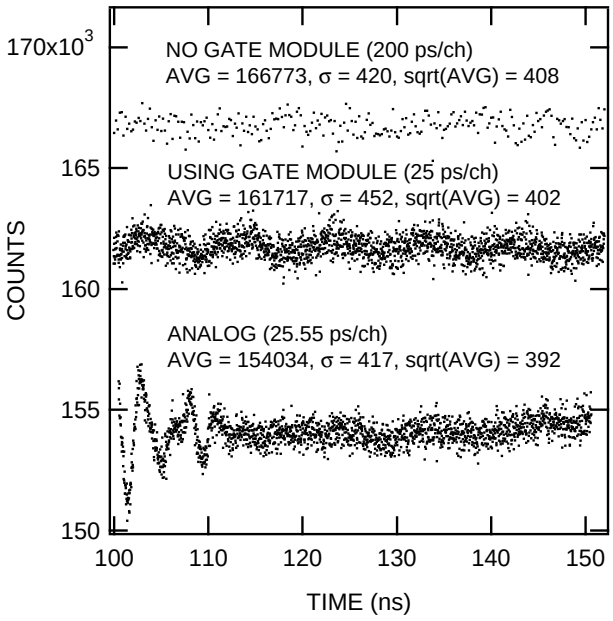

Figure 3.10: Linearity measurements of digital and analog positron lifetime spectrometers. The gate module is seen to cause ≈10 ns "oscillations". The data obtained without gate module has much wider bin widths in order to obtain similar statistical accuracy as with other methods. The averages and standard deviations presented in the figure are calculated between 115–145 ns. [Publ. II]

Second (ii), a gate module for detecting the coincidences is added to the previous setup for triggering the digitizer. This speeds up the measurement by reducing unnecessary data. The block diagram of this setup is presented in figure 3.9.

The results from linearity measurements are presented in figure 3.10: basic measurement without the gate module (i) shows good linearity. Using the gate module to speed up the measurement (ii) introduces "oscillations" with $\approx$ 10 ns periodicity. The explanation for these oscillations was not found. The amplitude of these oscillations is approximately of same magnitude as the nonlinearities of the analog spectrometer (which is used routinely in the HUT/Laboratory of Physics). These oscillations remain constant independent of the cable delays used in the measurement setup. They seem to have $\leq$ 2 ps effect on the average positron lifetime.

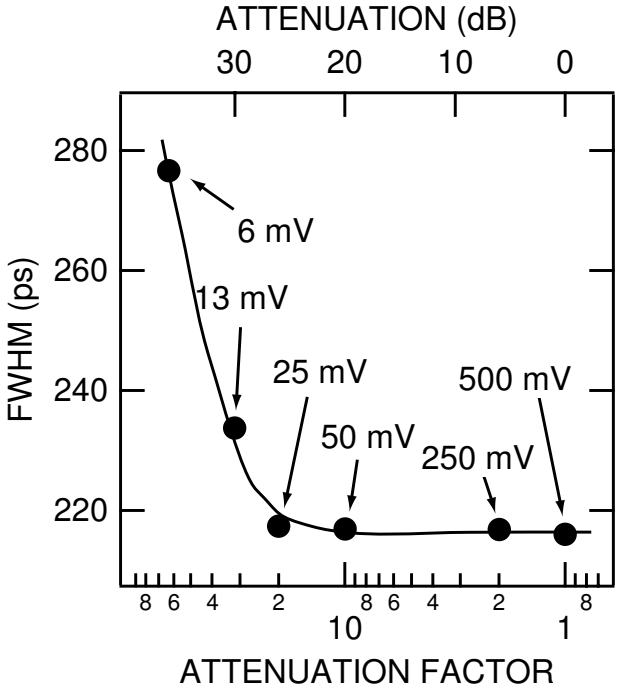

Figure 3.11: The time resolution as a function of anode pulse height at the digitizer input. The measurement has been performed by attenuating both the *start* and *stop* pulses. The voltages presented in the figure represent the lower level of the *stop* window. Only at the highest attenuations ($\geq$ 26 dB) the full scale range of the digitizer is not fully utilized. The width of the amplitude windows (50% ^{22}Na) has been kept constant in all measurements. The line is for guiding the eye. [Publ. III]

3.4.4 Performance with small pulse amplitudes

In positron lifetime spectrometers it is important to keep the average anode current in the PMTs as low as possible for good long-term stability of the system. [27] Therefore, operation of the spectrometer at low pulse amplitudes is advantageous. With modern CFDs the smallest pulses that can reliably be handled are some hundreds of mV in amplitude. Below this the operation may become unstable. The lowest full-scale range of DP210 is 50 mV which suggests that the internal noise level in the digitizer is much lower than this. The dependence of the pulse amplitude on the loss in time resolution was studied.

The study of the effect of reducing the anode pulse amplitudes was carried out by using attenuators between the pulse combiner and the digitizer (see figure 3.2). The full-scale range of the digitizer was chosen in each case such that the anode

pulses are digitized with maximum amplitude resolution. Fig. 3.11 illustrates the time resolution of the spectrometer as a function of the attenuation. The pulse amplitudes at the lower edge of the energy window of the stop detector are also marked in the figure. The resolution is constant at 218 ps until the LL amplitude decreases below 25 mV. With attenuation less than or equal to 26 dB, the anode pulses fill the whole full scale range of the digitizer. At higher attenuations, the quantization error increases and contributes to the worsening of the time resolution.

The effect of increasing the quantization error by truncating samples to artificially increase the quantization error was simulated. The results show that dividing the full scale range into 64 levels (6 bits) instead of 256 levels (8 bits), leads only to a 10-ps increase in the resolution. This effect is small compared to the increase from 218 ps (at 0 dB) to 275 ps at 36 dB attenuation corresponding to a similar decrease of the number of utilized voltage levels. Thus the degradation of the resolution is mainly due to the noise in the variable gain amplifier of the digitizer card.

The fact that the time resolution is close to optimum even when the smallest anode pulses are only 25 mV of amplitude means that the PMTs can be driven at average currents one tenth of those usually required with analog CFDs (usable pulses >250 mV). This decreases the degradation rate of the gain of the PMTs by the same factor, which again enhances the long-term stability of the spectrometer. When applying lower supply voltages over the PMTs, one just has to take care that the voltages at the input electron optics of the tubes are sufficiently high. [27] This usually means that one has to modify the voltage divider chain from the suggestions given by the manufacturer.

3.4.5 Stability

The medium-term stability the spectrometer was studied by measuring the position of the coincidence peak, as changes in both the true time zero ("offset") and in the time conversion ("gain") affect it. Repeated measurement of $\approx$ 110000 count ^{60}Co spectra for more than one week was performed. The positions of the coincidence peaks were then determined by fitting Gaussian functions. The spectrometer was located in an air-conditioned laboratory, whose temperature was 21–22 °C. The results of the measurements are shown in fig. 3.12. As can be seen from the figure, the magnitude of the time-zero drift of the spectrometer is $\approx$ 10 ps / week, which is a typical value also for analog spectrometers. [29] The drift of the analog spectrometers has been attributed primarily to the detectors and CFDs. [30] The similarity in the instabilities of the two types of spectrometers with totally different timing systems suggests that the instabilities originate from the detectors.

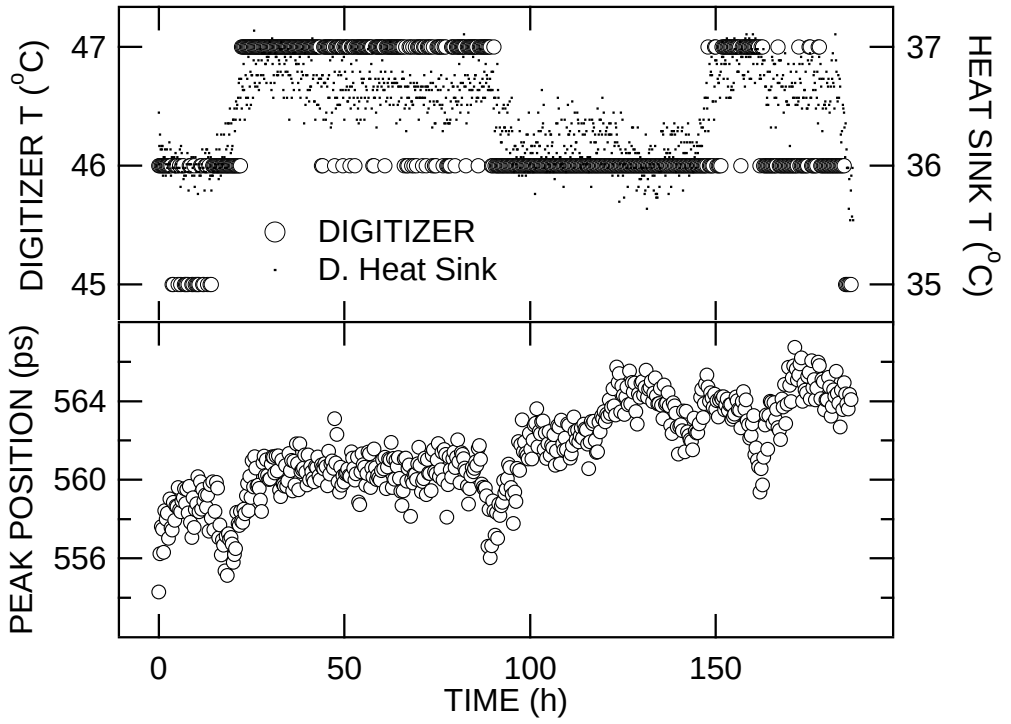

Figure 3.12: Stability measurement of the digital spectrometer. The peak positions have been obtained by measuring $\approx$ 110000 pulses from a ^{60}Co source. The temperatures are presented as reported by the digitizer [28] and as measured with a thermocouple connected to the heat sink of the digitizer (inside the measurement computer). The magnitude of the drift of the system is $\approx$ 10 ps/week, which is a typical value also for analog spectrometers. [Publ. IV]

One candidate for causing the drift is a change in the ambient temperature, also presented in fig. 3.12. The figure shows that the temperature and the drift of the spectrometer do not correlate strongly. Still, some similarities can be found—the temperature change coincidences with change in time-zero at least near 20 h and 90 h instants. Large temperature variations do cause drift—up to 20 ps changes in the time-zero, clearly due to temperature changes has been observed, when the spectrometer has been used in a non-airconditioned room.

3.5 Summary of construction of the digital positron lifetime spectrometer

In this thesis a digital positron lifetime spectrometer was constructed and its performance investigated extensively. The spectrometer was tested comprehensively and it was found that its performance characteristics are equal to that- or better than those of an analog system with similar detectors.

The price of the hardware of the digital system is already now lower than that of and analogue system. The time resolution of the constructed spectrometer was 220 ps, with $\Phi 30 \times 20$ mm^3 plastic scintillators, allowing count rates of 200 1/s under typical source activity and measurement geometry. The pulse processing part of the spectrometer is able to handle thousands of pulses per second, which is an order of magnitude more than the typical count rates. This opens also possibilities for high count rate applications, for instance measurements of long positron lifetimes with large scintillators (if positronium is present) or using the spectrometer in pulsed positron beams. The system can handle small anode pulses - down to 25 mV. The linearity and medium-term stability of the spectrometer were found to be similar to those of an analog spectrometer.

Chapter 4

Silicon Carbide (SiC)

Silicon carbide (SiC) is a semiconductor material for high-temperature, high-power, high-frequency and radiation resistant applications. Semi-insulating SiC has shown great potential as a substrate material for SiC- and III-nitride microwave applications. SiC substrates can be made semi-insulating by introducing deep levels (either impurities or intrinsic defects) to the material. The High-Temperature Chemical Vapor Deposition (HTCVD) technique [1] uses pure gases to grow high-purity semi-insulating SiC. Native vacancies have been observed in the material in electron paramagnetic resonance experiments,[1–5] but their role in the electrical compensation is unclear.

During the last few years SiC has been extensively studied using positron spectroscopy (see e.g. Refs. [31–47]). These studies often involve irradiated materials. Here positron lifetime spectroscopy is used to study as-grown bulk HTCVD 4H-SiC samples, grown under different conditions. The properties of this material can be expected to differ from those of the irradiated material.

4.1 General Properties

Silicon carbide is a crystalline solid. The material can crystallize to several (more than one hundred) different modifications, called polytypes. In all polytypes, each atom is tetrahedrally surrounded by four atoms of the other species, but the stacking sequence of the atom layers differ. The most commonly grown SiC polytypes are 3C, 4H and 6H. Here the polytypes are named using so-called Ramsdell notation, in which the number denotes the number of Si-C bilayers in one repeat unit and the letter denotes the symmetry, which may be cubic (C), hexagonal (H) or rhombohedral (R). For instance, if the three different layers are

Table 4.1: Some properties of typical SiC polytypes (Values presented at 300 K)

Poly-type	Stacking order	Hexag. [%]	Lattice Par. [Å]	Density [g/cm^3]	E_g [eV]	ϵ_0	ϵ_∞
3C	ABC	0	4.360	3.17	2.2 i	9.72	6.49
2H	AB	100	a 3.076	3.21	3.33 i		($\parallel$) 6.84
			c 5.048				($\perp$) 6.51
4H	ABCB	50	a 3.073	3.21	3.28 i	6H values	($\parallel$) 6.78
			c 10.053			used	($\perp$) 6.56
6H	ABCACB	33	a 3.081	3.21	2.86 i	($\perp$) 9.66	($\parallel$) 6.72
			c 15.117			($\parallel$) 10.03	($\perp$) 6.56

denoted A,B and C, the repeat units for layers in 3C is ABC, for 4H ABCB and for 6H ABCACB. Some of the properties of different SiC polytypes are presented in table 4.1.

SiC is a material not found in nature (exception to this are minute amounts found in some meteors). There are however many different methods available for growth of the material. SiC does not have a liquid phase in ordinary environments. Thus the Czochralski method commonly used for growing semiconductor crystals (e.g. Si) from liquid phase cannot be used for SiC. Because of this, SiC is normally grown directly from gas phase.

Polycrystalline SiC has been available for over a hundred years by so-called Acheson process. In the method SiC is produced by using electrical oven to heat coke and silica. SiC is then formed by sublimation at the cooler parts of the system.

The oldest method for growing single crystal bulk SiC is so-called Lely-method. In the method polycrystalline SiC is heated (at $\approx 2000-2500$ °C) in a crucible. The method allows growing of single crystals up to maximum size of approximately 2×2 cm^2. Typically these so-called Lely-platelets are of high quality, but the yield of this growth method is low and the polytype control nonexistent, hindering the use of the method for electronics applications commercially. When the Lely method is combined with the use of seed crystal, a physical vapor transport (PVT) method is obtained. Today wafers of diameter up to $\Phi = 100$ mm are commercially available. The PVT method is relatively simple, but this is also one of its drawbacks, in case the quality of the growth needs to be improved, there are only a limited set of parameters, which one can vary to improve the process. A new method for growing bulk SiC is High Temperature Chemical Vapor Deposition (HTCVD). In the method SiC is grown directly from high purity gases (methane and silane) above 1900 °C. [1] The gas-phase growth allows one to alter e.g. the C vs Si ratio.

In addition to bulk materials, thin epitaxial layers of high quality SiC can be

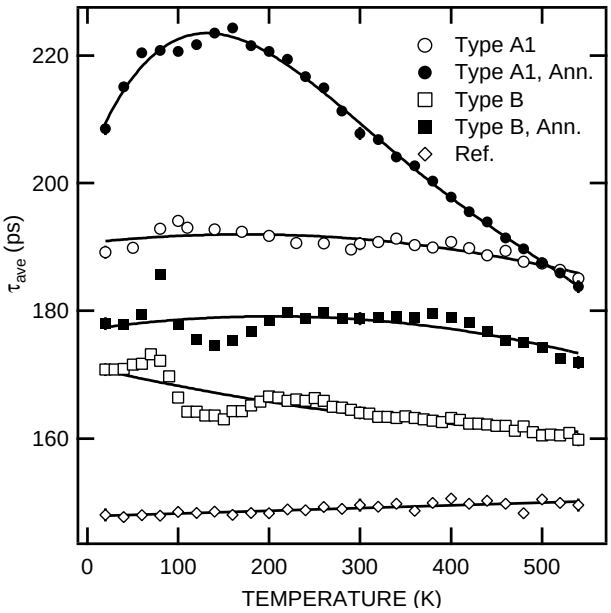

Figure 4.1: Average positron lifetime as a function of measurement temperature. The solid curves are used for calculation of τ_1^{TEST} (see eq. 2.3). [Publ. VI]

grown with molecular beam epitaxy (MBE) or chemical vapor deposition (CVD).

4.2 Samples and Positron lifetime measurements

The SiC samples studied in this thesis are undoped HTCVD grown material and their impurity levels are $< 10^{16}\mathrm{cm}^{-3}$ according to secondary ion mass spectrometry measurements [48],[Publ. VII] Post-growth annealings of the samples have been performed at 1600 °C in H_2 ambient in a CVD reactor. The samples and their annealing treatments are presented in table 4.2. Generally all as-grown samples are insulating but sample A1 shows weak n-type conductivity. After annealing the resistivity of A-type samples decreased and current-voltage measurements indicated that the samples became more n-type. The type B remain semi-insulating also after annealing. Preliminary results by Doppler broadening spectroscopy are shown in Publ. V.

Examples of positron lifetime spectra measured in the samples are shown in Fig 2.1. The reference sample, p-type bulk SiC, shows only a single lifetime of 150 ps, which is attributed for the positron lifetime τ_b in the SiC lattice. All HTCVD samples have more than one lifetime components.

Table 4.2: Samples, their annealing times (at 1600 °C in H_2 ambient), resistivities (at 300 K), positron lifetime values (measured at 300 K), positron trapping rates, vacancy concentrations and cluster sizes. Type A samples are grown in hydrocarbon rich and type B samples in hydrocarbon poor environment. The positron results include the measured average positron lifetime τ_{ave}, the fitted positron lifetime components $\tau_{\{1,2\}}$ and the intensity of the longer lifetime component I_2. The positron trapping rates to monovacancies κ_1 and to vacancy clusters κ_2, vacancy defect concentrations for V_{Si}-related defects [V_{Si}], vacancy clusters [V_N] and cluster sizes N have been determined by the positron annihilation measurements presented. Note that the change of Fermi-Level in type A2 evidently changes the charge state (and positron trapping coefficient) of the defects (concentrations in italic).

Sample, annealing time	Resistivity [Ω cm]	τ_{ave} [ps] ±0.5	τ_1 [ps] ±2	τ_2 [ps] ±10	I_2 % ±2	κ_1 [10^9 s^{-1}] ±20 %	κ_2	[V_{Si}] [10^{15} cm^{-3}] ±20 %	[V_N]	Cl. Size N [at.] ±20 %
A1	n-type	191	168	284	20	7.5	2.6	120	50	5
A1, 1h	n-type	208	138	350	33	2.1	2.9	30	28	10
A2	2×10^9	163	152	283	8	1.3	0.4	*61*	8	5
A2, 1h	1×10^8	183	146	406	14	1.4	0.9	*66*	6	16
A2, 2h	4×10^4 (n)	206	144	440	21	2.0	1.7	*33*	6	27
A2, 3h	5×10^2 (n)	216	144	451	24	2.4	2.1	*39*	6	32
B	$> 10^{10}$	164	150	261	13	1.3	0.6	61	15	4
B, 1h	$> 10^{10}$	179	146	342	17	1.4	1.0	69	11	9

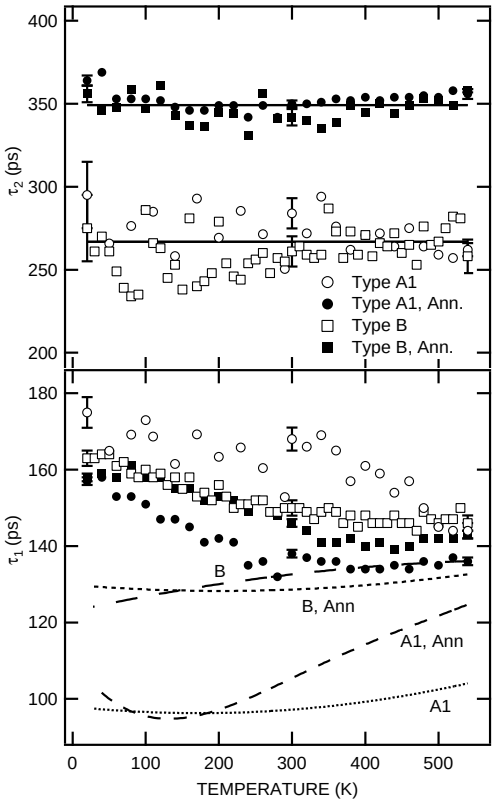

Figure 4.2: Positron lifetime components vs. measurement temperature. In the lower panel the lines present the parameter τ_1^{TEST} (Eq. 2.3), which gives information on the number of different vacancy defect species in the samples. [Publ. VI]

The lifetime spectra were decomposed into two components. Table 4.2 presents the average positron lifetime at 300K and the two separated components. The intensity of the longer component is also shown. The longer lifetime is 260-290 ps in the as-grown state and increases up to 450 ps after annealing. These lifetime values are typically associated to vacancy clusters consisting of more than two missing atoms.

The positron lifetime measurements as a function of temperature are shown in Fig. 4.1. The overall behavior of τ_{ave} in Fig. 4.1 resembles much of the behavior of the Doppler broadening S-parameter measured in publication V. The average lifetime above 200 K is constant or decreases with temperature. This shows that negative vacancies are present in the samples, since positron trapping to negative vacancies decreases with temperature, whereas trapping to neutral vacancies is

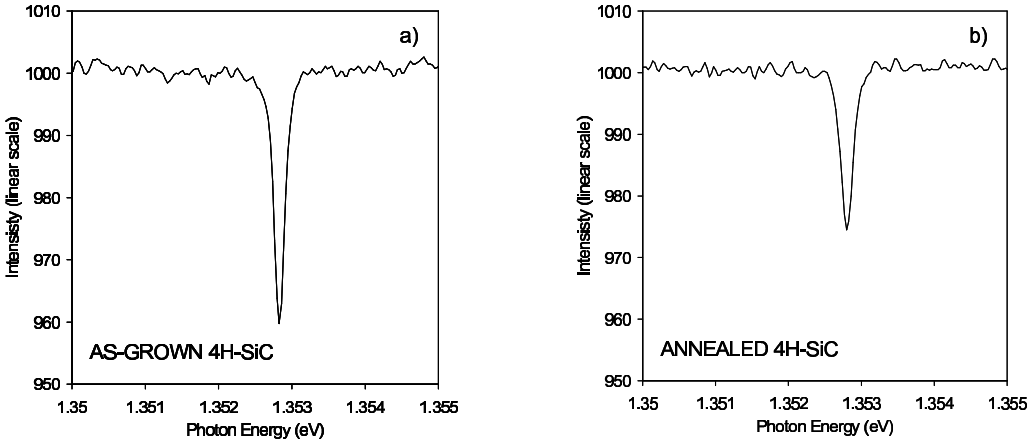

Figure 4.3: Optical transmission spectra of V_2-line corresponding to the V_{Si} before **a)** and after **b)** annealing. [Publ. VII]

temperature independent (see sect. 2.2). Below 200 K, especially well seen in the sample A1 Ann, the average lifetime starts to decrease, suggesting the presence of negative ions (residual impurities or intrinsic defects), which act as shallow traps for positrons. However, the concentrations of the shallow traps are low compared to those of the vacancy defects, as the decrease of the average lifetime is modest compared to the difference between the average and bulk lifetimes.

Fig. 4.2 shows the temperature dependence of the positron lifetime components. The positron lifetime at vacancy clusters τ_2 is approximately constant (350 ps or 270 ps) indicating positrons annihilating in a well-defined defect state in each sample. On the other hand, the shorter lifetime τ_1 has a clear tendency to decrease from 160-175 ps at 20 K to 140-150 ps at 500 K. If only the vacancy clusters corresponding to τ_2 were present in the samples, the lifetime τ_1 in the lattice would be related to τ_{ave}, τ_{b} and τ_2 as shown in equation 2.3.

The test lifetime τ_1^{TEST} calculated from the experimental values of $\tau_{\mathrm{ave}}, \tau_{\mathrm{b}}$ and τ_2 is shown in lower panel of figure 4.2. The calculated τ_1^{TEST} varies between 95-137 ps and thus it is well below the experimental τ_1 in all samples. This means that the vacancy clusters corresponding to τ_2 are not the only defects in the material. There exist also other smaller vacancy defects, which create a lifetime component mixed into the experimental τ_1 lifetime. The smaller defects are prominent at low temperatures and their concentration especially in the sample A1 grown under the hydrocarbon rich condition is high. The positron lifetime at the smaller vacancy defects is estimated to be above 170 ps from the low-temperature part of the Fig. 4.2. On the other hand, the τ_{ave} vs. T data (Fig. 4.1) indicates that the defect-specific lifetime is below 220 ps.

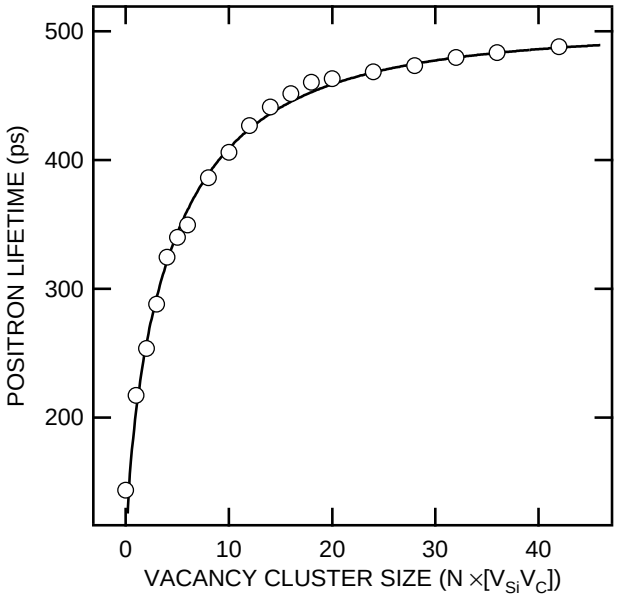

Figure 4.4: Calculated positron lifetimes in vacancy clusters in 4H SiC. The solid line is used for determining the cluster sizes from the measured τ_2. It is worth noticing that the sensitivity of the positron lifetime on the vacancy cluster size is significantly reduced when the cluster size exceeds 10 missing Si–C pairs. [Publ. VI]

4.2.1 Theoretical Positron lifetimes

In order to estimate the sizes of the observed vacancy clusters, positron lifetimes were calculated theoretically for vacancy clusters for 4H polytype. For the positron states the conventional scheme with the local density approximation (LDA) for electron-positron correlation effects and the atomic superposition method in the numerical calculations was used.[49, 50] The positron annihilation rate λ is

$$\lambda = \tau^{-1} = \pi r_0^2 c \int d\mathbf{r} \, |\psi_+(\mathbf{r})|^2 \, n_-(\mathbf{r}) \gamma[n_-(\mathbf{r})], \tag{4.1}$$

where n_- is the electron density, ψ_+ the positron wave function, r_0 the classical electron radius, c speed of light, and γ the enhancement factor. A modified Boronski-Nieminen enhancement factor,[51, 52] which takes into account lack of complete positron screening in semiconductors was used. The factor takes form

$$\begin{aligned}\gamma[n_-(\mathbf{r})] &= 1 + 1.23r_s + 0.8295r_s^{3/2} - 1.26r_s^2 \\ &\quad +0.3286r_s^{5/2} + (1 - 1/\epsilon_\infty)r_s^3/6, \end{aligned} \tag{4.2}$$

where r_s is calculated from the electron density as $r_s = \sqrt[3]{3/(4\pi n_-)}$. For the high-frequency dielectric constant in 4H polytype a value $\epsilon_\infty = 6.78$ was used. [53, 54]

The calculated clusters are formed by removing Si-C pairs from perfect lattice up to the size of 84 atoms. The atoms are removed according to their distance to the "origin" of the cluster (chosen to be the middle point between a Si-C bond, cubic position). The positron state is then solved in $480 - 2N$ atom supercells, where N is the number of Si-C pairs removed.

Because the atoms are simply removed from their ideal positions, the calculated clusters are non-relaxed. In general, the relaxation affects the open volume—and thus the positron lifetime of the clusters. Additionally, the presence of a trapped positron might alter the configuration of the surrounding atoms. According to calculations, lattice relaxations have been found to affect the positron lifetimes in case of V_2 in SiC by approximately 12 ps. [46, 55] However, the relative effect of relaxations in clusters have been found to be rather insignificant in clusters bigger than V_4 in silicon. [56]

The calculated positron lifetimes in the vacancy clusters are presented in Fig. 4.4. The results obtained are similar to those reported earlier for 3C and 6H SiC. [33] The calculated positron lifetime in bulk SiC is 144 ps, in agreement with the measured value 150 ps. When comparing the calculated and measured positron lifetimes in the vacancy clusters, the differences between the defects (clusters) τ_V and bulk τ_b lifetimes is compared.

4.3 Identification of the vacancy defects

4.3.1 Vacancy clusters

The measured lifetime τ_2 is longer than that determined earlier (typical values reported in literature are shown in parenthesis, see more discussion about lifetime values in section 4.3.2) for the carbon vacancy V_C ($\leq$160 ps), the silicon vacancy V_Si (180-210 ps), or divacancy ($<$ 250 ps) in SiC. The electron density in the defect is thus lower, indicating that the observed defects are vacancy clusters.

The comparison between the measured longer lifetime components and the theoretical calculations (section 4.2.1) can be used to estimate the sizes of the vacancy

clusters. According to the calculations (Fig. 4.4), a measured positron lifetime of 260 ps observed in as-grown samples corresponds to a vacancy cluster V_4 (2 Si–C molecules removed). The lifetime of 350 ps, detected after annealing, is expected for an open volume of a cluster V_{10}. The estimated cluster sizes in different samples are presented in Table 4.2. One can observe that the cluster sizes increase in the annealings from the size of roughly 5 missing Si–C pairs in the as-grown material up to 30 missing Si–C pairs in the A-type sample annealed for 3 hours. These approximate values represent the averages of the open volume distribution of vacancy clusters. This may mean various different cluster sizes or possibly a "magic" cluster size, in which the number of dangling bonds are minimized, as shown in e.g. Si and GaAs.[56, 57] Clustering of vacancies due to annealing has been previously reported in n-type 6H SiC after neutron- and ion irradiation. [42, 58, 59]

4.3.2 Si vacancy related defects

The estimated lifetime of the positrons trapped at the smaller observed vacancy defects is $\tau_V = 195 \pm 25$ ps range, *i.e.* $\tau_V - \tau_b = 20 \ldots 70$ ps. In order to identify this defect, one needs to consider the different lifetime values that have been associated with different aspects of SiC. Reported positron lifetimes (both experimental and theoretical) for bulk material range between 134 and 150 ps. The lifetime values associated with different vacancy defects vary clearly more.

For 4H polytype, bulk lifetime values including 141 ps [60], 145 ps [32] 150 ps [44], and for 3C-SiC 140 ps have been reported. [40] The most common polytype encountered in recent positron studies for SiC is 6H, for which several values for bulk lifetime have been proposed, in the range $136 \ldots 150$ ps. [31, 37–39, 41, 43–45] The theoretical calculations give lifetimes of 134 ps for 4H-SiC [46], 141 ps for 6H-SiC and 138 for 3C-SiC. [34] It should be noted that different calculation schemes (especially different enhancement factors) cause differences in the resulting absolute lifetimes, which becomes evident when comparing results from different studies. [46] Somewhat similar situation applies to experimental values (e.g. due to differences in measurement geometry, energy windows or source corrections). Thus, in comparisons between different lifetime values obtained from different studies, the differences between determined lifetime values in defects and bulk ($\tau_V - \tau_b$) are used, rather than solely the absolute values of the reported lifetimes.

The studies of positrons trapping in vacancy-type defects are typically performed by making use of irradiation, and the identification of the defects is often based on comparing the measured and the theoretical positron lifetime values. The reported values for positrons trapped by V_{Si} based on irradiation experiments

are typically around $\tau_V = 200$ ps, in the range $\tau_V - \tau_b = 14 \ldots 116$ ps. [31, 37, 38, 40, 45, 61] Theoretical calculations reported in the literature predict $\tau_V - \tau_b = 47 \ldots 64$ ps in 4H and 6H SiC [34, 46] for V_{Si}. For V_{C} values of $\tau_V - \tau_b = 8$ and 16 ps have been reported [37, 61] and theory gives $\tau_V - \tau_b = 6 \ldots 12$ ps. [34, 46]

In addition to the previous values, lifetime differences in the range $\tau_V - \tau_b = 65 \ldots 94$ ps have been reported in irradiated samples. [35, 43, 45, 47] The experimental values reported[31, 38] $\tau_V - \tau_b = 80 \ldots 83$ ps for the divacancy ($V_{\mathrm{Si}}V_{\mathrm{C}}$) are in good agreement with the reported theoretical predictions $\tau_V - \tau_b = 73 \ldots 75$ ps for 4H [46] and 6H [34] SiC.

Vacancies are commonly detected also in as-grown materials. In many cases the lifetime values are somewhat longer than the values found after irradiation. Lifetime values mainly in the range $250 \ldots 350$ ps ($\tau_V - \tau_b = 100 \ldots 200$ ps) have been observed in as-grown SiC samples. [36, 37, 39, 44] Also smaller values of $\tau_V - \tau_b = 50 \ldots 75$ ps have been reported [41] and attributed to V_{Si} and $V_{\mathrm{Si}}V_{\mathrm{C}}$. According to theoretical calculations reported earlier [33] and in this thesis (section 4.2.1), a lifetime of 250 ps corresponds to open volume at least of a similar size with that of V_4, *i.e.* $(V_{\mathrm{Si}}V_{\mathrm{C}})_2$.

In the light of the lifetime values discussed previously, the possible candidates for the smaller vacancy defects observed here are thus monovacancies or monovacancy related complexes in the Si and C sublattices and small clusters with at most 2–3 missing atoms. Several arguments point in the direction that these defects are related to V_{Si} rather than V_{C}. The main point is that, as shown above, the lifetime of the smaller vacancy defect is $\geq$170 ps, *i.e.* above all presented estimates for the carbon vacancy V_{C}. In addition, the C vacancy in semi-insulating SiC could be positively charged according to theoretical calculations [55] and EPR experiments [5] and thus repulsive to positrons. Hence, the defect responsible for the increase of τ_1 at low temperature is a Si vacancy or a complex involving V_{Si}. This conclusion is in agreement with the EPR and infrared absorption results,[1, 4, 5] which suggest that samples similar to A1 contain V_{Si}, whereas samples of type B have positive C vacancies, and also V_{Si} but less than in a sample like A1. Furthermore, absorption measurements [Publ. VII] show the decrease of the signal associated to the V_{Si} in annealing (Fig. 4.3).

It is interesting that the Si vacancy related defects are prominent at low temperatures, whereas the larger vacancy clusters dominate the positron lifetime spectrum at high measurement temperatures. Positron trapping at neutral defects is independent of temperature, whereas the negative defects become stronger positron traps at lower temperatures. Hence, the temperature dependence of the lifetime components suggests that the Si vacancy related defects act as acceptors in SI HTCVD SiC, but the vacancy clusters are electrically neutral. In annealed A1 type sample, however, the average positron lifetime decreases with the in-

creasing temperature. This means evidently that also a part of the clusters in the n-type material are negatively charged.

4.4 Vacancy defect concentrations

The vacancy defect concentrations were estimated from the positron trapping model using the decomposed lifetimes and intensities. In the calculation it is assumed that both vacancy clusters (CL) and vacancies in Si-sublattice (V) are present and the positron lifetimes at the vacancies in the Si-sublattice and in the bulk SiC are intermixed to the component τ_1. Equations 2.5 and 2.6 are used to calculate the positron trapping rates κ in clusters κ_{CL} and in V_{Si}-related defects κ_{V}. The positron lifetime for the vacancy cluster is taken directly from the decomposition as $\tau_{\mathrm{CL}} = \tau_2$. For the positron lifetime at the Si vacancy related defects $\tau_{\mathrm{V}} = 195$ ps is used. The value is in the middle of the range determined for the lifetime of the smaller defect. Values close to this are also often attributed for the positron lifetime in V_{Si} (see section 4.3.2). The defect concentrations are obtained from the trapping rates κ as $c = \kappa\ N_{\mathrm{at}}/\mu$. Here $N_{\mathrm{at}} = 9.64 \times 10^{22}$ cm^{-3} is the atomic density of SiC.

A positron trapping coefficient of $\mu_{\mathrm{V}}^{-} = 2 \times 10^{15}$ s^{-1} for singly negative vacancies at 300 K in Si sublattice is used. This is a typical value in wide band-gap semiconductors. [7] For neutral vacancies the value $\mu_{\mathrm{V}}^{0} = 1 \times 10^{15}$ s^{-1} (see section 2.2) is used. In n-type samples the value $3\mu_{\mathrm{V}}^{-}$ is used, since theoretical calculations predict that V_{Si} changes its charge state from 1^- to 2^-, and eventually to 3^-, when the Fermi level approaches the conduction band. [55] This change of charge state of V_{Si} is likely to occur in the samples A2, where conductivity of the samples changes from semi-insulating to n-type conductive, indicating the movement of the Fermi level. For small vacancy clusters (transition limited positron trapping), the positron trapping coefficient for vacancy clusters of n vacancies can be approximated as $\mu_{\mathrm{CL}} = n\mu_{\mathrm{V}}$. [62] As can be observed in Fig. 4.1, a part of the vacancy clusters in the annealed sample A1 are likely to be negative, which increases the overall trapping coefficient of the clusters. Hence the trapping coefficient of the vacancy clusters in the annealed sample A1 is probably somewhat underestimated. The determined vacancy defect concentrations are summarized in Table 4.2.

The experimental vacancy defect concentrations and sizes (Table 4.2) suggest the following interpretation: Annealings of the samples of type A, grown under hydrocarbon rich conditions, increase the sizes of the vacancy clusters from approximately 5 to 30 vacancies, with a simultaneous decrease of the cluster concentration. This suggests that smaller clusters are disintegrated in the annealing

and larger clusters are formed via migration. The concentration of the Si vacancy related complex is also lowered by the annealing of the n-type sample A1. This is in agreement with the observation presented in [Publ. VII], in which the optical absorption signal related to V_{Si} was found to decrease due to annealing. Interestingly, the increase of the total open volume of the clusters is of the same order of magnitude with the volume lost from V_{Si}-related defects. Thus it seems that annealing causes V_{Si} to accumulate to the vacancy clusters by migration.

In the originally semi-insulating sample A2, the trapping rate κ_1 of positrons to the V_{Si}-related defects increases roughly by a factor of two. However, the annealing decreases the resistivity of the sample towards n-type conductivity, which indicates that the Fermi level moves towards the conduction band. This is likely to induce an increase of the negativity of the V_{Si}, which would increase the trapping coefficient to these vacancies by a factor of 2–3, depending on the initial and final charge states. Hence, when taking into account the change of the charge states of the defects, the concentration of the V_{Si} seems to decrease during the annealing. It should be noted, though, that since the exact charge states of the defects are not known, the concentration estimates for the V_{Si}-related defects in this sample are somewhat unreliable.

Annealing increases the average size of the vacancy clusters also in the sample of type B, grown under hydrocarbon poor conditions. The concentration of the V_{Si}-related defects is not significantly changed in the annealing either.

4.5 Electrical compensation

The temperature dependence of the average positron lifetime (Fig. 4.1) shows that the samples of both types A and B do not contain significant concentrations of negative ions, such as impurities or negative interstitials or antisite defects. These types of defects thus contribute little to the electrical compensation, at maximum at the level of their detection limit; their concentration is at most in the mid-10^{15} cm^{-3} range. This observation correlates also with low concentrations of boron and aluminium acceptors ($< 5 \times 10^{15}$ cm^{-3} and $< 5 \times 10^{14}$ cm^{-3}, respectively [48]) and other impurities [Publ. VII] measured with secondary ion-mass spectrometry.

The samples grown in hydrocarbon rich conditions (type A) are either slightly n-type already after the growth, or lose their high resistivity after annealing. The detected negative V_{Si}-related complex is an obvious candidate for the compensating intrinsic defect in as-grown material. Hence the n-type character of the annealed A-type samples can be explained by the loss of compensation due to loss of negative V_{Si} to primarily neutral vacancy clusters. It is worth noticing

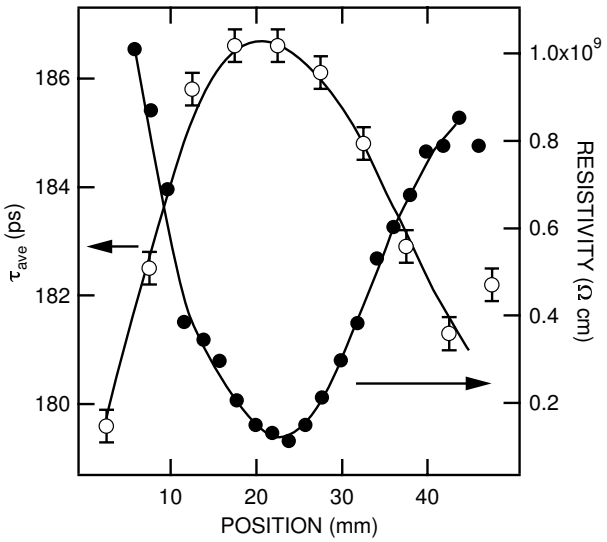

Figure 4.5: Average positron lifetime and resistivity as a function of position on the diameter of a 2" type A wafer. The lines are for guiding the eye. [Publ. VI]

that a part of the vacancy clusters turn negative in the annealing of the sample A1. This does not affect the interpretation that the compensation is weakened due to the migration of V_{Si} to the clusters, however, as the negativity implies that the cluster concentration presented in Table 4.2 might overestimate the "proper" value.

The concentration of the vacancy clusters should thus increase with the decreasing resistivity of HTCVD SiC. To verify this relation in the as-grown samples, the positron lifetime and resistivity were measured as a function of position in a strip like sample, cut diagonally across a wafer grown in hydrocarbon rich growth conditions (type A). The lifetime component $\tau_2 = 247 \pm 10$ ps remained constant over the sample, indicating constant vacancy cluster size (≈ 4 atoms). As can be seen in Fig. 4.5, the average positron lifetime and the resistivity of the sample anticorrelate. The change of τ_{ave} is caused by the variation in the intensity I_2 and thus the positron trapping rate at the vacancy clusters. The concentration of the clusters thus decreases with increasing resistivity of the material, most likely since less compensating V_{Si}-related complexes have migrated to the neutral vacancy clusters during the growth.

The annealing of samples grown under hydrocarbon poor conditions (type B) leads to growth of the vacancy clusters, but the concentration of the smaller defects is not substantially changed. This suggests that in B-type material the Si vacancies have transformed to (or are combined to form) more stable complexes, such as the $V_{\mathrm{C}}\mathrm{C}_{\mathrm{Si}}$ [63, 64] or $V_{\mathrm{Si}}V_{\mathrm{C}}$ [6], which remain as compensating centers

after the annealing. It is quite possible that the high resistivity of type B samples is dominated by the C vacancy,[2, 3, 5, 65] which is more stable than V_{Si} according to calculations.[64, 66]

4.6 Summary of experiments in SiC

In this thesis high purity semi-insulating High Temperature Chemical Vapor Deposition (HTCVD) grown silicon carbide was studied primarily using positron lifetime spectroscopy. Vacancy clusters and smaller vacancy-type defects were found in the material. The sizes of the observed clusters were estimated and it was found that in the as-grown material the cluster sizes were approximately 4-5 atoms and in the annealed material up to 30 atoms. The presence of the clusters is shown to anticorrelate with the electrical resistivity of the material. The smaller vacancy defects are shown to be negative and their open volume is shown to be larger than that of V_{C} in the hydrocarbon rich material. Thus they are identified as V_{Si} related defects. Their concentration is estimated to be in the $10^{16}..10^{17}$ cm^{-3} range. It is suggested that the observed V_{Si}-related defects act as compensating defects and their migration to the clusters leads to loss of resistivity.

Chapter 5

Summary

In this thesis a digital positron lifetime spectrometer has been designed, set up and tested comprehensively. Also, positron lifetime spectroscopy has been used to study defects in High Temperature Chemical Vapour Deposition (HTCVD) grown semi-insulating silicon carbide (SiC).

The digital system consists of a fast commercial digitizer connected to a computer, a simple coincidence circuit and software to extract the timing from the collected detector pulses. The system has the same time resolution as a conventional analog apparatus using the same detectors. The pulse processing part of the spectrometer is able to analyze and store in real time several thousands of events per second, which is an order of magnitude more than the count rates in typical positron lifetime experiments. The data acquisition can handle small pulses, down to a few tens of millivolts, and its time scale linearity and stability are very good.

Positron spectroscopy was used to study native vacancy defects in High Temperature Chemical Vapor Deposition grown high purity semi-insulating silicon carbide. The material was shown to contain (i) vacancy clusters consisting of 4–5 missing atoms and (ii) Si vacancy related negatively charged defects. The growth of the measured cluster size due to the annealing of the samples was observed. The total open volume bound to the clusters is found to anticorrelate with the electrical resistivity both in as-grown and in annealed material. The measurements show that the Si vacancy related defects compensate electrically the as-grown material. They are suggested to migrate to increase the size of the clusters during annealing, leading to loss of resistivity.

Bibliography

[1] A. Ellison *et al.*, Proc. of MRS fall meeting 2000 **640**, H1.2 (2001).

[2] M. E. Zvanut and V. V. Konovalov, Applied Physics Letters **80**, 410 (2002).

[3] V. V. Konovalov, M. E. Zvanut, and J. van Tol, Physical Review B **68**, 012102 (2003).

[4] N. T. Son, Z. Zolnai, and E. Janzén, Physical Review B **68**, 205211 (2003).

[5] N.T. Son *et al.*, Materials Science Forum **433-436**, 45 (2003).

[6] N. T. Son *et al.*, Physical Review Letters **96**, 055501 (2006).

[7] R. Krause-Rehberg and H. Leipner, *Positron Annihilation in Semiconductors: Defect Studies*, *Springer Series in Solid-State Sciences* (Springer-Verlag, Berlin, Heidelberg, New York, 1998).

[8] K. Saarinen, P. Hautojärvi, and C. Corbel, in *Identification of Defects in Semiconductors*, edited by M. Stavola (Academic Press, N.Y., 1998).

[9] P. Hautojärvi and C. Corbel, in *Positron Spectroscopy of Solids*, Vol. CXXV of *Proceedings of the International School of Physics "Enrico Fermi"* (North Holland publishing company, Amsterdam, New York, Oxford, 1993).

[10] P. Mascher, S. Dannefaer, and D. Kerr, Physical Review B **40**, 11764 (1989).

[11] J. Mäkinen, P. Hautojärvi, and C. Corbel, J. Phys. Condens. Matter **4**, 5137 (1992).

[12] K. Saarinen *et al.*, Physical Review B **39**, 5287 (1989).

[13] P. Simões, J. Martins, and C. Correia, IEEE Transactions on Nuclear Science **43**, 1804 (1996).

[14] J. L. Arcos, E. Garcia-Torano, P. Olmos, and J. Marin, Nuclear Instruments & Methods A **353**, 251 (1994).

[15] D. Cussans and H. Heath, Nuclear Instruments & Methods A **362**, 277 (1995).

[16] A. Codino, Nuclear Instruments & Methods A **440**, 191 (2000).

[17] H. Saito *et al.*, Nuclear Instruments & Methods A **487**, 612 (2002).

[18] H. Saito and T. Hyodo, Radiation Physics and Chemistry **68**, 431 (2003).

[19] H. Saito and T. Hyodo, Physical Review Letters **90**, 431 (2003).

[20] F. Becvar, J. Cizek, I. Prochazka, and J. Janotova, Nuclear Instruments & Methods A **539**, 372 (2005).

[21] P. Bevington and D. Robinson, *Data Reduction and Error Analysis for the Physical Sciences* (McGraw-Hill, New York, 2003).

[22] *Numerical Recipes in C++: The art of Scientific Computing*, 2nd ed. (Cambridge University Press, Cambridge, New York, Melbourne, Madrid, Cape Town, 2002).

[23] C. de Boor, *A Practical guide to splines* (Springer-Verlag, New York, Berlin, 1978).

[24] K. Rytsölä *et al.*, Applied Surface Science **194**, 260 (2002).

[25] B. Somieski, T. Staab, and R. Krause-Rehberg, Nuclear Instruments & Methods A **381**, 128 (1996).

[26] *Model 566 Time-to-Amplitude Converter Operation and Service manual*, EG&G Ortec, Oak Ridge, Tennessee, USA, 1984.

[27] J. Nissilä, K. Rytsölä, K. Saarinen, and P. Hautojärvi, Nuclear Instruments & Methods A **481**, 548 (2002).

[28] A. A. Rothenberg, Private communications, 2004, Offset of the thermometer of the particular digitizer is apparently off by ≈ 10 °C.

[29] J. Nissilä *et al.*, Nuclear Instruments & Methods A **466**, 527 (2001).

[30] I. MacKenzie, in *Proc. of the International School of Physics "Enrico Fermi", Course LXXXIII, Varenna, Italy 1981*, edited by W. Brandt and A. Dupasquier (North-Holland Publishing Company, Amsterdam, New-York, Oxford, 1983), Vol. 14-24, p. 220.

[31] S. Arpiainen *et al.*, Physical Review B **66**, 075206 (2002).

[32] W. Bauer-Kugelmann, G. Kögel, P. Sperr, and W. Triftshäuser, Materials Science Forum **255-257**, 662 (1997).

[33] G. Brauer *et al.*, J. Phys. Condens. Matter **10**, 1147 (1998).

[34] G. Brauer *et al.*, Physical Review B **54**, 2512 (1996).

[35] G. Brauer *et al.*, Physical Review B **54**, 3084 (1996).

[36] D. Britton *et al.*, Applied Physics Letters **78**, 1234 (2001).

[37] S. Dannefaer, D. Craigen, and D. Kerr, Physical Review B **51**, 1928 (1995).

[38] L. Henry *et al.*, Physical Review B **67**, 115210 (2003).

[39] A. Kawasuso, H. Itoh, S. Okada, and H. Okumura, Journal of Applied Physics **80**, 5639 (1996).

[40] A. Kawasuso *et al.*, Appl. Phys. A **67**, 209 (1998).

[41] C. Ling, A. Deng, S. Fung, and C. Beling, Appl. Phys. A **70**, 33 (2000).

[42] A. Mokrushin, A. Girka, and A. Shiskin, Phys. Stat. Sol. A **128**, 31 (1991).

[43] A. Polity, S. Huth, and M. Lausmann, Physical Review B **59**, 10603 (1999).

[44] W. Puff *et al.*, Appl. Phys. A **61**, 55 (1995).

[45] A. Rempel and H.-E. Schafer, Appl. Phys. A **61**, 51 (1995).

[46] T. Staab, L. Torpo, M. Puska, and R. Nieminen, Materials Science Forum **353-356**, 533 (2001).

[47] A. Uedono *et al.*, Japanese Journal of Applied Physics **37**, 6650 (1997).

[48] A. Ellison *et al.*, Materials Science Forum **433-436**, 33 (2003).

[49] M. Puska and R. Nieminen, J. Phys. F **13**, 333 (1983).

[50] M. Puska and R. Nieminen, Reviews of Modern Physics **66**, 841 (1994).

[51] E. Boronski and R. Nieminen, Physical Review B **34**, 3820 (1986).

[52] M. Puska, J. Phys. Condens. Matter **3**, 3455 (1991).

[53] P. Shaffer, Applied Optics **10**, 1034 (1971).

[54] H. Mutschke *et al.*, Astron.Astrophys **245**, 187 (1999).

[55] L. Torpo, M. Marlo, T.E.M. Staab, and R. Nieminen, J. Phys. Condens. Matter **13**, 6203 (2001).

[56] T. E. M. Staab, M. Haugk, T. Frauenheim, and H. S. Leipner, Physical Review Letters **83**, 5519 (1999).

[57] D. Chadi and K. Chang, Physical Review B **38**, 1523 (1988).

[58] W. Anwand, G. Brauer, D. Pankin, and W. Skorupa, MSF **363-365**, 442 (2001).

[59] W. Anwand *et al.*, Applied Surface Science **194**, 127 (2002).

[60] S. Dannefaer, V. Avalos, and R. Yakimova, Materials Science Forum **483-485**, 481 (2054).

[61] S. Dannefaer and D. Kerr, Diamond and Related Materials **13**, 157 (2004).

[62] R. Nieminen and J. Laakkonen, Appl. Phys. **20**, 181 (1979).

[63] T. Lingner *et al.*, Physical Review B **64**, 245212 (2001).

[64] M. Bockstedte, A. Mattausch, and O. Pankratov, Physical Review B **69**, 235202 (2004).

[65] N. T. Son *et al.*, Materials Science Forum **457-460**, 437 (2004).

[66] E. Rauls, T. Frauenheim, A. Gali, and P. Deak, Physical Review B **68**, 155208 (2003).